Gondwana Research 97 (2021) 240–262

Contents lists available at ScienceDirect

Gondwana Research

journal homepage: www.elsevier.com/locate/gr

Jurassic fast polar shift rejected by a new high-quality paleomagnetic pole from southwest Greenland

Evgeniy V. Kulakov [a,*], Trond H. Torsvik [a,b], Pavel V. Doubrovine [a], Trond Slagstad [c], Morgan Ganerød [c], Petter Silkoset [a], Stephanie C. Werner [a]

[a] Centre for Earth Evolution and Dynamics (CEED), University of Oslo, PO Box 1028, Blindern NO-0315, Norway
[b] School of Geosciences, University of Witwatersrand, Johannesburg 2050, South Africa
[c] Geological Survey of Norway, Trondheim, Norway

ARTICLE INFO

Article history:
Received 8 January 2021
Revised 17 May 2021
Accepted 30 May 2021
Available online 2 June 2021
Handling Editor: Joseph Meert

Keywords:
True Polar wander
Paleomagnetism
Southwest Greenland
Late Jurassic
Global Apparent Polar Wander Path

ABSTRACT

A selective compilation of paleomagnetic data from North America indicates that a vast amount of rapid polar motion occurred in Late Jurassic time. The over 30° polar shift that accumulated during a relatively short time interval (~160–145 Ma) suggests an episode of fast true polar wander (TPW) and was referred to as the Jurassic "monster polar shift" by some workers. However, this rapid TPW event is not supported by paleomagnetic data on a global scale. Here, we scrutinize the Jurassic apparent polar wander path (APWP) by virtue of a new paleomagnetic and $^{40}Ar/^{39}Ar$ geochronology study of Mesozoic coast-parallel dykes exposed in southwest Greenland. Combined with existing geochronological data, our results show that the dykes were emplaced during a prolonged period centered at 147.6 ± 3.4 Ma (2σ). A primary nature of the characteristic remanent magnetization is supported by multiple positive baked contact tests and a reversal test. The paleomagnetic pole calculated from 40 site-mean paleomagnetic directions is located at P_{lat} = 69.3°**S**, P_{long} = 5.0°E (A_{95} = 4.6°), or at P_{lat} = 73.9°**S** and P_{long} = 0.4°E when reconstructed to North America. Our new high-quality paleomagnetic pole and an updated global APWP do not support the fast Jurassic polar shift but instead indicate steady polar motion with moderate rates of about 0.7°/Myr. The new pole effectively reduces the mismatch between the APWPs for Laurentia and Europe. Our critical reassessment of the monster polar shift indicates that it may be an artifact of paleomagnetic and geochronological data that were previously used to argue for its existence.

1. Introduction

Paleomagnetism, the study of the Earth's magnetic field recorded in rocks, has long served as the principal tool for deciphering paleogeography and the long-term variations of the geomagnetic field. Paleomagnetic signals, initially retrieved from rocks by measuring natural remanent magnetization (NRM) are commonly converted into paleomagnetic poles using a geocentric axial dipole field model. A series of paleomagnetic poles of different ages can then be used to construct apparent polar wander paths (APWPs), which represent a convenient way to illustrate the apparent motion of the pole relative to a fixed continent. This polar motion reflects plate motion, rotation of the entire solid Earth with respect to the spin axis (true polar wander, TPW), or a combination of these two processes.

APWPs are traditionally used to infer relative positions and motions of different continents and to construct paleogeographic models. The robustness of these models intrinsically depends on the quality of the paleomagnetic poles used to assemble the APWPs. Although a vast amount of paleomagnetic data have been accumulated since the dawn of paleomagnetism in the 1950s, a number of important problems remain unsolved. One of these long-lasting problems is the well-known discrepancy between the Late Jurassic – Early Cretaceous APWPs for Laurentia (North America and Greenland) and Europe (e.g., Van der Voo, 1992; Courtillot et al., 1994). Laurentian paleomagnetic poles, the vast majority of which come from North America, systematically plot at lower latitudes compared to the coeval poles from Europe (Fig. 1a) and Gondwana, resulting in equivocal paleogeographic models. The APWP mismatch cannot be explained by the uncertainties in relative plate reconstructions. One potential reason for the discrepancy may be the inclusion of a large number of poles from the Colorado Plateau, which has not been tectonically

* Corresponding author.

https://doi.org/10.1016/j.gr.2021.05.021
1751-7311/

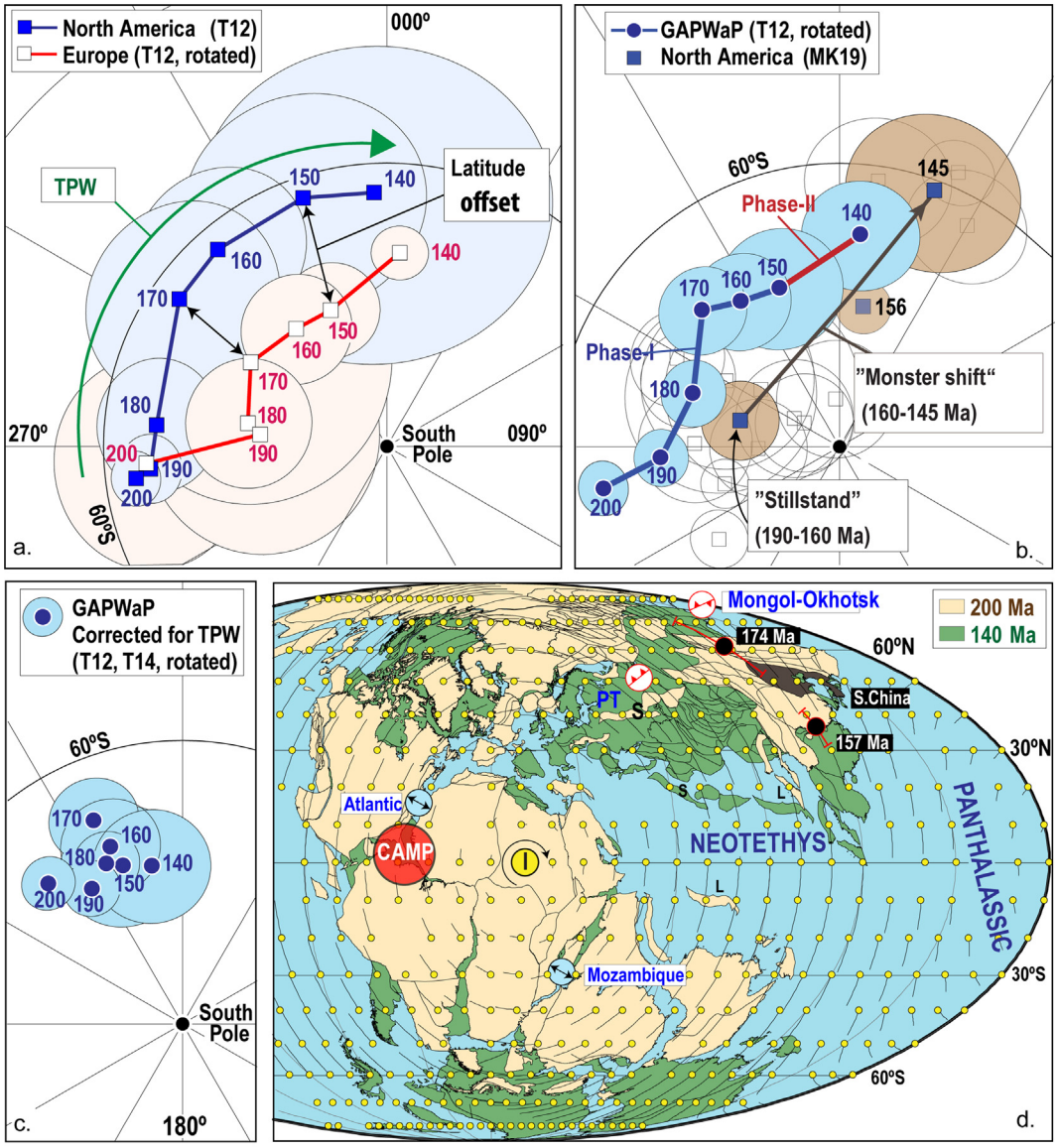

Fig. 1. Apparent polar wander paths (APWPs) and global paleogeography between 200 Ma and 140 Ma. **(a),** Running-mean APWPs with window length 20 Myr for Laurentia (including poles from the Colorado Plateau) and Europe (rotated to North American frame) with sedimentary poles corrected for potential inclination shallowing (Torsvik et al., 2012; T12). Note the *latitude offset* between the two APWPs. A second feature to notice is the systematic easterly polar shift during the Jurassic and Early Cretaceous, which amounts to ~42° and ~27°of cumulative APW (great-circle distances) for North America/Laurentia and Europe, respectively. This shift is dominated by true polar wander, TPW (Steinberger and Torsvik, 2008; Torsvik et al., 2012, 2014; Torsvik, 2019). **(b),** 'The global APWP (GAPWaP) of Torsvik et al. (2012; T12) shown in North American coordinates and compared with the North American poles selected by Muttoni and Kent (2019). They argued for an APW "standstill" between 190 and 160 Ma (pole #1 in Table 1) followed by a fast (*2.1°/Ma*) easterly shift of about *31°* between 160 and ~ 145 Ma. The 145 Ma pole is the mean pole reported in Muttoni and Kent (2019; pole #5 in Table 1); gray poles with unfilled A_{95}s (partly coved by our shaded ovals) are the paleomagnetic poles used by Kent and Irving (2010) to calculate the "standstill" and the mean 145 Ma poles (poles ## 42–53 and 39–41 in *table 5* of Kent and Irving 2010 for the standstill and 145 Ma, respectively); **(c),** The GAPWaP corrected for TPW i.e. counter-clockwise rotations at velocities of 0.45°/Ma (190 and 150 Ma) and 0.8°/Ma between 150 and 140 Ma (Torsvik et al., 2012, 2014). All poles are plotted in orthogonal south polar projection. **(d),** Global paleogeographic reconstructions between 200 Ma (pale yellow shading) and 140 Ma (green shading). The difference between the two maps is to a large extent attributed to a phase of clockwise TPW centered on an equatorial axis of 11°E (marked I). TPW motions are shown as black lines connected to yellow dots with the sense of motion from the yellow dot toward the tail (see Torsvik et al., 2012 for details). Differential plate motion (continental drift) between 200 and 140 Ma was associated with, for example, the opening of the Central Atlantic and Mozambique Basins between East and West Gondwana, and subduction of the Paleotethys (PT) and the Mongol-Okhotsk Ocean. East Asia and the Cimmerian terranes (e.g. Sanand, S) and Lhasa (L) were not parts of core Pangea at 200 Ma. Some of these terranes were drifting northward and approaching Eurasia whilst the entire globe was experiencing clockwise TPW. The marked locations in North China that correspond to 164 and 157 Ma (based on Yi et al., 2019) were argued to represent TPW, but the magnitude and velocity are not supported from the global reconstructions.

coherent with North America. Furthermore, the Colorado poles are overwhelmingly represented by data from clastic sedimentary rocks, which are often prone to record paleomagnetic inclination shallower than that of the ambient magnetic field, a phenomenon known as inclination shallowing (King, 1955, Løvlie and Torsvik, 1984; Tauxe and Kent, 1984, 2004; Tauxe et al., 2008; Kodama, 2009). Correcting these data for inclination shallowing leads to a better agreement between the coeval APWP segments for North America and Europe/Gondwana (Torsvik et al., 2012) but does not fully solve the aforementioned APWP problem.

The APWPs of Torsvik et al. (2012) show a pronounced and systematic easterly shift from the Early Jurassic (200 Ma) to the Early Cretaceous (140 Ma). Observed not only in North American data (Fig. 1a) but also in the global APWP (GAPWaP in Fig. 1b), this ~41° shift is dominated by TPW (Fig. 1c) as the bulk continents show a clockwise rotation around an equatorial location near 11°E (Fig. 1d; Steinberger and Torsvik, 2008; Torsvik et al., 2012; 2014). Originally, Steinberger and Torsvik (2008) suggested a single phase of steady TPW between 195 and 145 Ma, but based on refined APWPs, Torsvik et al. (2012) modelled TPW between 200 and 140 Ma as two separate phases with an accelerated TPW rate during the 150–140 Ma interval (Fig. 1b).

Kent and Irving (2010), Kent et al. (2015) and most recently Muttoni and Kent (2019) have constructed alternative APWPs (Fig. 1b) using different selection criteria and excluding all paleomagnetic poles from the Colorado Plateau. Their global APWP yields slightly higher pole latitudes in North American coordinates than the GAPWaP of Torsvik et al. (2012), but more importantly, all three studies argued for a pole standstill between 190 and 160 Ma followed by a fast easterly shift between 160 and 145 Ma (Fig. 1b). This shift of about 31° of great circle distance was interpreted as TPW at an average rate of ~2°/Myr and dubbed the "monster polar shift" by Kent and co-workers. The 156 Ma pole (Table 1), which is based on data from two kimberlite localities in Ontario province, Canada (Kent et al., 2015), was described by Muttoni and Kent (2019) as "bridging the gap" between the mean 190–160 Ma standstill and the 145 Ma poles. The 190–160 Ma standstill was defined by 12 poles (two poles from North America and the remaining from South America, Australia, South Africa and East Antarctica), four of which have an identical 183 Ma age. The 145 Ma pole is constrained by three individual paleomagnetic poles from North America, Africa and Svalbard. The nominal polar wander rates amount to 4.3°/Myr, and 1.3°/Myr between 160 and 156 Ma and 156 and 145 Ma, respectively, if the 156 Ma pole is included in the TPW calculations. We note that the 145 Ma mean pole (Fig. 1b, Table 1) includes a pole from the Svalbard Hinlopenstretet dolerites (Halvorsen, 1989). The age assigned to this pole is based on the results of the K/Ar age estimate of 144 Ma (Gayer et al., 1966; Burov et al., 1977). However, more recent studies (Nejbert et al., 2011; Corfu et al., 2013; Polteau et al., 2016) indicate that most Svalbard Dolerites, including the Hinlopenstretet intrusions are significantly younger (124–119 Ma).

Muttoni and Kent (2019) argued that the monster polar shift was supported by paleomagnetic poles from Adria (after correction for potential inclination shallowing), but this conclusion is based on the assumption that Adria has remained tectonically coherent with Africa since the deposition of the Adrian sedimentary sequences. The assumed tectonic coherence is at best unlikely, as documented by the complicated tectonic history of Adria for the past 200 Myrs (up to 20° of counterclockwise rotation and 5 mm/year of present-day northward motion) and the lack of stability relative to both northeast Africa and Europe (e.g. Van Hinsbergen et al., 2014, 2020; Le Breton et al., 2017).

In a recent attempt to test for rapid TPW using paleomagnetic data from the oceanic domain, Fu and Kent (2018) reported statistically indistinguishable (at the 95% confidence level) paleolatitudes for the Pacific plate between ~165 and 135 Ma, which *per se* do not lend any additional support to the monster polar shift. For further details, we refer readers to an overview of the Mesozoic Pacific-Panthalassic evolution in Torsvik et al. (2019). The most recent study that addressed the rapid Jurassic polar motion (Fu et al., 2020), reported two new paleomagnetic poles from the La Negra volcanics in Northern Chile (Table 1). The statistically similar paleomagnetic poles dated to 165.8 ± 1.8 and 152.8 ± 0.8 Ma were compared with the group of ~145 Ma poles used in the studies of Kent et al. (2015) and Muttoni and Kent (2019), including the much younger Hinlopenstretet pole. Although this study also advocated for an episode of fast TPW during the Jurassic, the associated average polar wander rate of 1.21° ± 0.35°/Myr (Fu et al., 2020) was significantly slower than those proposed in earlier studies.

In addition to the 160–145 Ma TPW "monster shift", an episode of large and fast TPW during the Jurassic has been argued to occur between 174 ± 6 Ma and 157 ± 4 Ma, causing a rapid southward displacement of ~25° (Fig. 1d) for the Eastern Asian blocks (Yi et al., 2019) and triggering what is known as the Great Jurassic East Asian Aridification event. Both shifts are compatible with a clockwise TPW rotation, but the timing is distinct for these two episodes and both of them are also different from the more gradual and slower TPW suggested by the GAPWaP of Torsvik et al. (2012) (Fig. 1b).

Overall, the Jurassic monster polar shift is defined by paleomagnetic poles that are not consistent with each other and thus suggest very different rates of polar motion. The reliability of some of the poles may be questioned because of the potential for bias, for example, introduced by non-averaged paleosecular variations (kimberlite poles) or the lack of tectonic coherence of studied rocks with a reference continent (poles from Adria and the Colorado Plateau). In addition, the younger ~145 Ma bound for the proposed Jurassic polar shift is defined by only *three* paleomagnetic poles, which do not agree with each other. In order to address the controversial Jurassic APW and conflicting estimates of potential TPW rates, we turned our attention to the Late Jurassic – Early Cretaceous coast-parallel dykes in southwest Greenland, which are unambiguously tectonically coherent with cratonic Greenland. Paleomagnetic results from these dykes have been previously reported by Fahrig and Freda (1975), who published a paleomagnetic pole (P_{lat} = 56°N, P_{long} = 168°E, A_{95} = 6.0°) based on data from eight sites, representing five individual dykes and combined with data from 23 samples of Ketelaar (1963). In the same year, Piper (1975) published paleomagnetic results from a more extensive sample collection, sampled approximately 200 km to the south from the localities of Fahrig and Freda (1975). Natural remanence of both polarities, measured from studied dykes, yielded a paleomagnetic pole (P_{lat} = 72°N, P_{long} = 191°E, dp/dm = 6.2/7.5°, N = 13) that differed substantially from that of Fahrig and Freda (1975). The difference between the paleomagnetic poles may stem from the much more limited number of dykes studied by Fahrig and Freda (1975), perhaps not sufficient to average out paleosecular variations of the geomagnetic field, but can also be related to different laboratory protocols. Fahrig and Freda (1975) essentially used a blanket demagnetization to 25–30 mT peak alternating fields, whereas Piper (1975) utilized multiple-step demagnetization with significantly stronger peak fields of up to 80 mT. Based on K-Ar data available at the time, Fahrig and Freda (1975) and Piper (1975) assigned their paleopoles Late Triassic and Middle Jurassic ages, respectively.

In this contribution we present a new paleomagnetic pole obtained from samples of 40 dykes from the coast-parallel dyke swarm of southwest Greenland. We demonstrate the primary (thermoremanent) nature of NRM in these samples through multiple baked contact tests and a reversal test. Based on published U-Pb, Rb-Sr, $^{40}Ar/^{39}Ar$ radiometric dates and the results of new $^{40}Ar/^{39}Ar$ geochronology analyses reported here, we assign a Late Jurassic (147.6 Ma) nominal mean age for the emplacement of the studied dykes and discuss the implications of our new paleomagnetic pole for estimates of polar motion during the Late Jurassic and Early Cretaceous. We also present updated APWPs for Europe and North America and an updated global APWP for this time interval.

Table 1
Selected paleomagnetic poles, discussed in the text and shown in Figs. 1, 10, 11 and 12.

Pole	Cont./Plate	Age (Ma)		A_{95} (°)	P_{lat} (°S)	P_{long} (°E)	E_{lat} (°N)	E_{long} (°E)	E_{ang} (°)	N_{am} P_{lat} (°S)	N_{am} P_{long} (°E)	Fig.	Reference
1	N. America	190–160	Standstill (mean)	4.0						79.5	284.8	1,11,12	Muttoni and Kent (2019)
2		~175–169	Moat Volcanics	7.4						78.7	270.3	10, 11	van Fossen and Kent (1990)
3		156	Ontario kimb.	2.8						75.5	9.5	10	Kent et al. (2015)
4		146.4 ± 1.2	Ithaca kimb.	3.8						58.0	23.1	10,11, 12	van Fossen and Kent (1993)
5		145 ± 2	Mean poles 4, 14 & 15b	9						61.2	20.2	1,10	Muttoni and Kent (2019)
6		120.4 ± 1	Alfred Complex	3.6*						74.0	29.8		McEnroe (1996a)
7		120.6 ± 0.4	Cape Neddick	4.6*						75.6	353.8		McEnroe (1996a)
8		~122	White Mountains	6.9						71.9	7.4		Van Fossen and Kent (1992)
9		122 ± 3	Tatnic Complex	4.6*						65.7	28.4		McEnroe (1996a)
10		124 ± 1	Monteregian Hills	2.0*						72.0	11.2		Foster & Symons (1979)
11		125 ± 3	Lebanon Diorite	7.5*						73.3	14.3		McEnroe (1996a)
12		122 ± 4	Mean poles 6–11	4.3						72.5	15.3		This study
13	Greenland	147.6 ± 3.4	SW Gr.Dykes	4.6	69.3	5.0	67.5	−118.5	−14.0	73.9	0.4	10,11,12	This study
14	Svalbard	124–119	Hinlopen. Dolerites	7.5	66.0	20.0	69.0	154.8	−23.1	60.6	10.9	11a	Halvorsen et al. (1990)
15	S. Africa	145	Swartuggen-Bumbeni	6.3	31.7	104.3	64.8	−16.8	−63.5	57.6	46.9	11a	Hargraves et al. (1997)
15b		145	Swartuggen-Bumbeni	6.3	31.7	94.3				63.1	29.6	11a	Kent and Irving (2010):Erroneous
16		134 ± 2	Etendeka Lavas	6.3	47.5	88.9	64.9	−16.7	−60.3	70.9	19.8		Owen-Smith et al. (2019)
17		134 ± 2	Etendeka Lavas	3.5	49.1	87.6	64.9	−16.7	−60.3	72.2	15.7		Dodd et al. (2015)
18		134 ± 2	Mean poles 16–17, 24–27	1.4						72.5	12.7	10c	This study
	S. America												
19	-Colorado	165.8 ± 1.8	La Negra N.	7.6	84.3	180.9	−76.1	327.0	41.4	76.1	327.0	10b	Fu et al. (2020)
20	-Parana	157.6 ± 3	Zapican Dykes	7.2	86.4	178.9	−75.1	334.8	40.0	75.1	334.8	10b	Cervantes-Solano et al. (2020)
21	-Patagonia	155 ± 3.5	Chon Aike Ignim.	8.6	84.3	191.3	−76.5	335.9	34.8	76.5	335.9	10b	Gonzales et al. (2019)
22	-Colorado	152.8 ± 0.8	La Negra S.	10.8	84.5	76.4	−70.1	358.5	79.1	70.1	358.5	10b	Fu et al. (2020)
23		154.5 ± 1.9	Mean poles 3, 20–22	6.0						74.8	350.5	10c	This study
24	-Amazonia	134 ± 2	Parana (Brazil)	2.4*	83.0	71.4	32.2	83.3	−17.2	72.1	11.1		Ernesto et al. (1999)
25	-Amazonia	134 ± 2	Central Parana	2.5*	84.1	69.2	32.2	83.3	−17.2	72.6	7.7		Owen-Smith et al. (2019)[recalc]
26	-Parana	134 ± 2	Parana (S. Brazil)	1.1	84.4	111.6	29.4	86.7	−19.4	74.1	11.4		Owen-Smith et al. (2019)[recalc]
27	-Parana	134 ± 2	Parana (N. Uruguay)	4.2	84.8	95.8	29.4	86.7	−19.4	72.7	9.5		Solano et al. (2010)
28	Italy (Adria)	158	Bomb pre-CM30⁑	4.3	56.8	86.5	63.1	−13.2	−75.9	76.4	305.0	11b	M2013, Muttoni and Kent (2019)
29		158	Foz pre-CM30⁑	3.7	64.8	74.9	63.1	−13.2	−75.9	71.3	274.5	11b	M2013, Muttoni and Kent (2019)
30		150 ± 6	Mean (N = 4)⁑	4.3	37.3	89.6	62.4	−14.7	−72.6	65.8	3.8	11b	M2013, Muttoni and Kent (2019)
31		143	VFF CM17-CM21⁑	3.1	45.3	83.5	62.5	−14.5	−70.0	70.0	347.3	11b	M2013, Muttoni and Kent (2019)
32	N. China	174 ± 6	Nandaling Fm.	9.1	65.9	320.3	69.0	154.8	−23.6	68.2	317.5	12b	Yi et al. (2019)
33		157 ± 4	Tiaojishan/Lanqi Fm.	5.1	66.1	28.8	69.0	154.8	−23.3	59.9	17.4	12b	Yi et al. (2019)
34	Colorado	156 (strat)	L. Morrison Fm.⁑	5.3*	66.6	−11.0	34.6	254.6	5.0	62.5	−9.0	11c	Steiner and Helsley (1975)
35		150 (strat)	U. Morrison Fm.⁑	3.6*	67.3	20.0	34.6	254.6	5.0	63.9	17.7	11c	Steiner and Helsley (1975)
36		148 (strat)	U. Morrison Fm.⁑	4.1*	68.7	14.0	34.6	254.6	5.0	65.1	12.2	11c	Bazard and Buttler (1994)

Notes: All Euler rotation to used to rotate poles to North American coordinates are after Torsvik et al. (2012), except poles 28–31 that combines with Adria-NE Africa rotation parameters of Van Hinsbergen et al. (2020) and poles 34–36 where the Colorado Plateau data have been adjusted for a 5°rotation (Bryan and Gordon, 1986). Note that North China was considered as an integral part of Eurasia by Yi et al. (2019), which may not be true (see text and Fig. 1d). **A_{95}** – 95% confidence circle of the corresponding paleomagnetic pole (*α_{95}); P_{lat} and P_{long}, paleomagnetic pole latitude and longitude, respectively; Nam P_{lat} and Nam P_{long} are paleomagnetic pole latitude and longitude in the North America reference frame. E_{Lat}, E_{lon}, E_{ang} – Euler rotation parameters: latitude, longitude and rotation angle, respectively; *strat* – estimated age of the sedimentary rocks, based on stratigraphic position or/and available fauna; ⁑ Sedimentary rocks have been corrected for potential inclination flattening: For Adria this is variable (M2013 - Muttoni et al., 2013) but we have used a flattening factor f = 0.6 for Colorado Plateau poles and when calculating the APWP.

2. Geology, geochronology, and sampling

The Mesozoic dykes in southwest Greenland are exposed approximately 400 km along the Greenland coast between ~64°N and 60°N (Fig. 2). The dykes were emplaced into a Precambrian (Archean) basement between ~150 and 135 Ma (Table 2) in response to crustal stretching (pre-drift extension) during the earliest stages of the Labrador Sea and Davis Strait formation (Larsen et al., 2009). U-Pb and Rb-Sr analyses of the presumed oldest dykes (Larsen et al., 2009) yielded a series of ages ranging between 152.1 ± 1.6 and 149.8 ± 1.2 Ma, and one less-precise Rb-Sr age of 156 ± 14 Ma. Further increase in regional stress and melting of upwelling asthenospheric mantle led to emplacement of a slightly younger, Early Cretaceous set of dykes, which yielded $^{40}Ar/^{39}Ar$ ages between 134.9 ± 1.4 and 141.5 ± 2.2 Ma (recalculated from Larsen et al., 1999; 2009 using updated decay constants and calibrations of Renne et al., 2010). The Jurassic-Cretaceous dykes exhibit wide compositional variation ranging from mafic compositions (tholeiitic basalt, enriched or transitional basalt, alkali basalt, and phonolite) and lamprophyres (monchiquite) to ultramafic varieties

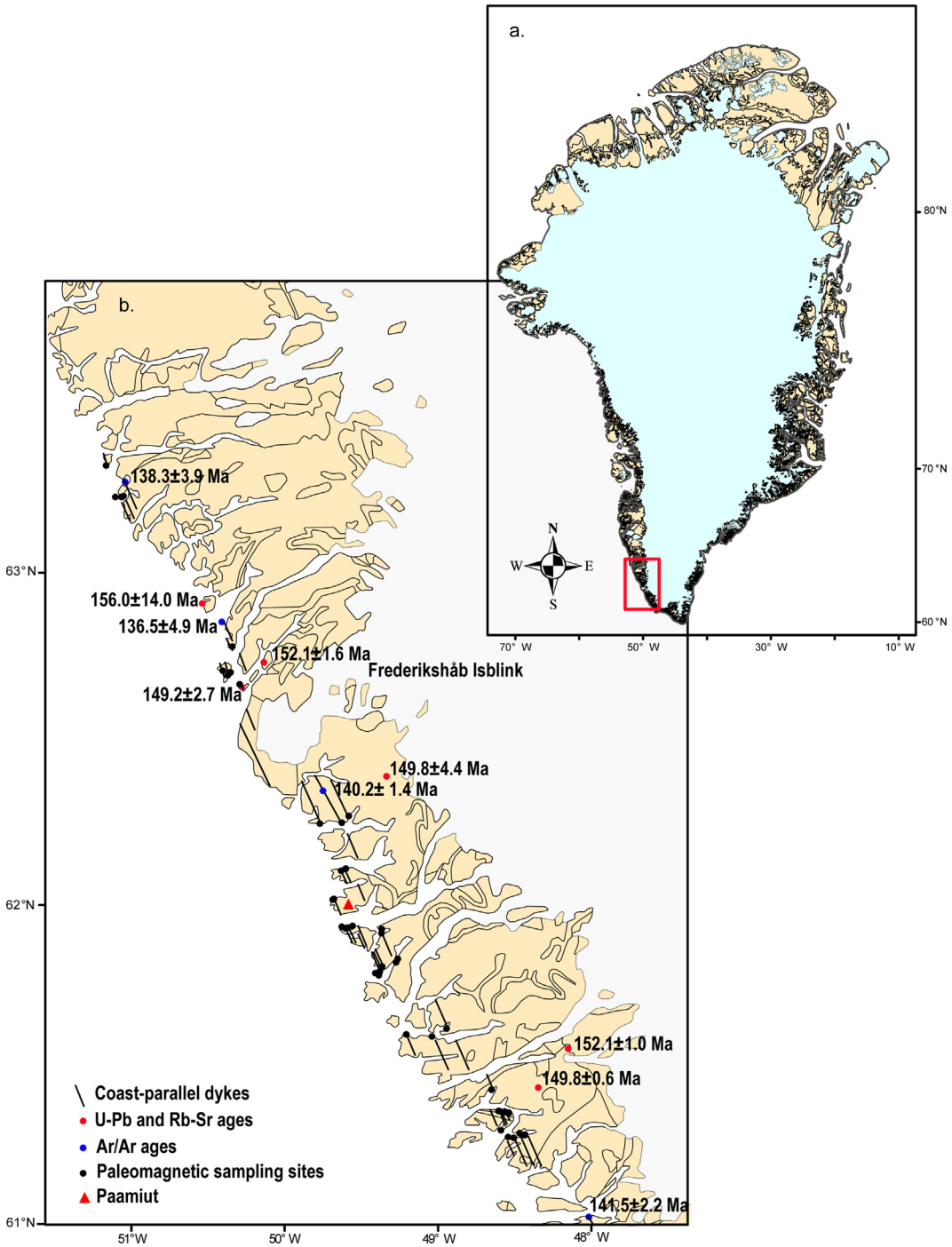

Fig. 2. Study area and sampling locations. **(a),** Simplified map of Greenland showing our study area, and **(b),** a map of the study area showing the distribution of sampling sites, available radiometric ages and schematic distribution and orientation of the Late Jurassic and Early Cretaceous coast-parallel dykes. Red triangle indicates the town of Paamiut.

Table 2
Summary of available radiometric ages for coast-parallel dikes from southern West Greenland. Notes: Lat and Long – sampling sites coordinates; rock type according to Le Maitre (2002), modified by Tappe et al. (2005); N – number of consecutive steps used to determine the plateau age. % Ar – a total percent of ^{39}Ar release during heating steps. * - ^{40}Ar/^{39}Ar ages of Larsen et al. (1999, 2009), recalculated using updated calibrations from Renne et al. (2010). Original ages are shown in parenthesis. Site ID (e.g. GL26) in parentheses indicates the corresponding paleomagnetic site in this study.

Locality	Lat. (°) N	Long. (°) E	Rock name	Method	Age, Ma ± 2σ	Source
Sanerut	61.0379	−48.0132	Basalt	*Ar-Ar	*141.5 ± 2.2 (141.1)	Larsen et al., 2009
Qaarsuarsuk	60.8301	−47.0211	Basalt	*Ar-Ar	134.9 ± 1.4 (133.3)	Larsen et al. 1999
N of Paamiut (GL77)	62.3387	−49.7127	Basalt	*Ar-Ar	140.2 ± 1.4 (138.6)	Larsen et al. 1999
Pyramidefjeld	61.4249	−48.2904	Aillikite	U-Pb	149.8 ± 0.6	Larsen et al., 2009
Midternæs	61.5425	−48.1235	Aillikite	U-Pb	152 ± 1 0.0	Larsen et al., 2009
Frederikshåb Isblink	62.7267	−50.1094	Alnöite	U-Pb	152.1 ± 1.6	Larsen et al., 2009
Frederikshåb Isblink	62.3830	−49.3670	Monchiquite	Rb-Sr	149.8 ± 4.4	Larsen et al., 2009
Frederikshåb Isblink	62.8763	−50.5539	Monchiquite	Rb-Sr	156 ± 14.0	Larsen et al., 2009
Frederikshåb Isblink (GL81)	62.6577	−50.2781	Monchiquite	Rb-Sr	149.2 ± 2.7	Larsen et al., 2009
N of Frederikshåb Isblink (GL26)	63.2692	−51.0515	Basalt	Ar-Ar	138.3 ± 3.9	This study
Frederikshåb Isblink (GL84)	62.8155	−50.3927	Basalt	Ar-Ar	136.5 ± 4.9	This study

such as melilite and aillikite, and carbonatite (see Larsen et al., 2009 for further details). The dykes were emplaced into the coast-parallel NW-SSE oriented and now steeply seaward-dipping system of fractures that were formed and tilted due to crustal stretching and subsequent rifting of Greenland from North America (Watt, 1969; Larsen et al., 2009). All sampled dykes are subvertical and, with the exception of a few instances, dip WNW at angles between 90° and 75°-70° (Supplementary material).

For this study, we collected 6–12 oriented core samples from 41 paleomagnetic sites, representing 38 individual dykes (Fig. 2b, Table 3), including those dated to 140.2 ± 1.4 and 149.2 ± 2.7 Ma (Larsen et al., 2009, our paleomagnetic sites GL 77 and GL81, respectively). In addition, we collected 14–18 samples from four dykes and their baked and unbaked host-rocks for paleomagnetic baked contact tests. Samples were collected using a gasoline-powered portable paleomagnetic drill and oriented using a magnetic compass, checked with sun compass and/or back-azimuth transit readings. Block samples for geochronology were collected from the interiors of dykes sampled for paleomagnetism.

3. Results

3.1. ^{40}Ar/^{39}Ar geochronology

Four samples, representing four individual dykes were analyzed for their ^{40}Ar/^{39}Ar isotopic composition (see Supplementary material for details, Supplementary Data, Table S1), and ^{40}Ar/^{39}Ar isotope analyzes were performed at the geochronology laboratory of the Geological Survey of Norway (Trondheim). Consistent with the results of the previous studies (Larsen et al., 1999, 2009), our samples were very difficult to date. Except for biotite crystals from two samples, which yielded ages of 138.3 ± 3.9 Ma (GL 26) and 136.5 ± 5.0 Ma (GL 84), (Fig. 3, Table 2), all measured clinopyroxene, hornblende, and plagioclase crystals had massive excess argon and yielded either erroneously old ages or uninterpretable data. In addition, samples from seven dykes were used in an attempt to extract suitable minerals for U-Pb age determinations (zircon or baddeleyite), but no datable grains of these minerals have been found in these samples.

3.2. Rock-magnetism and paleomagnetism

Rock-magnetic characteristics and natural remanent magnetization (NRM) of dykes were measured at the Ivar Giæver Geomagnetic Laboratory, University of Oslo. We used at least two representative samples per site to examine the rock magnetic properties. Thermomagnetic measurements (low-field magnetic susceptibility versus temperature curves) were made using an AGICO MFK1-FA magnetic susceptibility meter equipped with a high-temperature furnace and a cryostat. The thermomagnetic κ (T) curves were measured upon cycling from −194 °C to room temperature, followed by high-temperature heating-cooling cycles from room temperature to typically 600 °C (or sometimes to 700 °C) and back to room temperature in an inert atmosphere (argon). For the majority of samples, the κ(T) curves were reversible or nearly reversible and revealed the presence of a magnetic phase with Curie temperatures in a range of 560 °C to 575 °C, indicating magnetite to low-Ti titanomagnetite as a magnetic carrier (Fig. 4a, b, d-f, Supplementary material). The presence of a characteristic peak at ~−153 °C, associated with the Verwey transition (Verwey, 1939) further suggests the presence of nearly stoichiometric magnetite.

Samples from several dykes yielded highly irreversible thermomagnetic curves (Fig. 5c), indicating complex magnetic mineralogy and severe heating-induced mineralogical changes. These κ(T) dependences revealed the presence of magnetic minerals with Curie temperature in a range between 150 and 400 °C, interpreted as titanomagnetite with varying Ti contribution and the presence of another magnetic phase with Curie temperature of ~550 °C, likely titanomagnetite with lower Ti content. On cooling, these samples exhibited a shift of Curie temperatures towards significantly lower values (Fig. 4c) as well as an increase of susceptibility of the high-temperature magnetic phase (Fig. 4c inset). This increase was accompanied by a slight shift of Curie temperature towards more magnetite-like temperatures (~580 °C). While the reason for such mineralogical transformation is difficult to ascertain, we speculate that the observed behavior can be explained by heating-induced formation of a higher-Ti phase and magnetite (low-Ti phase) due to an incomplete, in this case, unmixing of initial homogeneous titanomagnetites.

Magnetic hysteresis parameters (coercivity, H_c; coercivity of remanence, H_{cr}; saturation remanent and saturation moments, M_{rs} and M_s) were measured using a Lake Shore PMC MicroMag 3900 Vibrating Sample Magnetometer (VSM). All hysteresis loops have regular shapes and indicate the presence of low to intermediate coercivity magnetic minerals (Fig. 5a-d, Supplementary material). The hysteresis parameters suggest pseudo-single domain (PSD) magnetic carriers in all samples (Fig. 5a-e). M_{rs}/M_s ratios, when plotted against the ratios of coercivities (H_{cr}/H_c) (Day et al., 1977), fall perfectly along the single-domain–multidomain mixing curves for magnetite (Dunlop, 2002), further indicating that magnetite and/or low-Ti titanomagnetites are the principle ferromagnetic phases in the most of studied samples (Fig. 5e).

NRM of all samples was measured using an AGICO JR-6A spinner magnetometer hosted in a MMLFC low-magnetic-field cage.

Paleomagnetic samples were stepwise thermally or alternating field (AF)-demagnetized using a MMTD80A automatic, microprocessor-controlled thermal demagnetizer and an AGICO LDA5 AF demagnetizer, respectively. Progressive demagnetization (typically 12–16 steps) was carried out until the NRM intensity of the specimens fell below noise level or until the measured remanence directions became erratic and unstable. NRM components were isolated using principle-component analysis (Kirschvink, 1980).

The majority of the samples showed demagnetization of a two-component NRM. Secondary components, characterized by variable directions, were typically removed at temperatures of 150–300 °C (Fig. 6 f, g) or in alternating fields of 5–8 mT (Fig. 6 d). Well-defined characteristic NRM components (ChRM) with a straight linear decay to the origin of the vector endpoint diagrams, were usually unblocked in a range of temperatures between ~550 and 575 °C or by AF demagnetizations of 50–65 mT (Fig. 6); this further indicates that the principle remanence carriers are low to intermediate-coercivity magnetite and low-Ti titanomagnetite. Samples characterized by titanomagnetites with greater titanium content, revealed during thermomagnetic analyses, lost most of their remanence by heating to temperatures not exceeding 500 °C (Fig. 6 c).

Site-mean paleomagnetic directions were calculated using Fisher statistics (Fisher, 1953). A site-mean direction was accepted if calculated from at least three individual sample directions and with an associated 95% confidence circle (α_{95}) not exceeding 15°. Paleomagnetic data from 43 sites (40 individual dykes) met our data-acceptance criteria. Paleomagnetic data from two sites were rejected due to erratic demagnetization behavior that resulted in uninterpretable vector endpoint diagrams.

Baked contact tests performed on samples from four individual dykes and their host-rocks indicate a primary origin of natural remanence. Fig. 7 shows two examples of baked contact tests. Sam-

Table 3
Summary of paleomagnetic data.

Site ID	Lat (° N)	Long (° E)	N	Dg (°)	Ig (°)	Ds(°)	Is(°)	α_{95}(°)	k	P_{lat} (°S)	P_{long}(°E)
GL25^{BC}	63.2954	−51.1899	8	352.4	69.9	352.4	69.9	3.0	351.0	79.7	334.8
GL26$^{Ar/Ar.\ 138.3}$	63.2692	−51.0515	5	156.0	−54.9	156.0	−54.9	3.4	518.8	58.5	348.3
GL27	63.2242	−51.1062	10	351.4	66.4	9.1	61.3	3.5	268.2	68.5	290.3
GL28	63.2240	−51.0656	5	284.9	67.2	303.5	75.1	10.8	51.0	64.8	61.9
GL29	63.2266	−51.0525	4	342.4	62.4	332.8	62.6	6.1	229.1	65.3	0.8
GL42	61.2811	−48.5432	8	154.0	−60.5	162.9	−61.0	2.7	435.5	68.2	347.5
GL43	61.2789	−48.5070	9	312.8	65.8	357.0	67.3	3.4	228.6	78.7	321.3
GL44^{BC}	61.3025	−48.5910	10	291.9	64.2	325.4	70.7	2.3	453.0	70.9	37.7
GL47	61.2867	−48.4358	8	326.9	63.3	349.7	56.0	5.2	113.2	64.4	331.0
*GL49 + 46	61.3231	−48.4846	18	330.3	64.4	349.9	64.9	2.4	202.3	74.4	338.0
*GL50 + 45	61.3265	−48.5154	16	345.2	77.9	356.1	77.2	2.2	274.6	85.4	110.9
GL51	61.3617	−48.5965	9	132.1	−64.6	144.8	−66.3	3.1	283.4	66.6	24.9
GL52	61.3623	−48.6054	6	158.7	−42.9	166.9	−45.2	6.2	129.0	54.3	331.7
GL53^{BC}	61.4293	−48.6508	10	142.3	−61.3	151.6	−61.0	1.6	923.8	64.2	5.7
GL54	61.6191	−48.9444	9	295.2	67.4	295.2	67.4	1.7	888.9	53.7	53.3
GL56	61.5949	−49.0392	8	130.2	−64.5	130.2	−64.5	3.0	353.5	58.0	35.8
GL57	61.6005	−49.2072	9	298.1	76.2	282.9	73.3	2.5	427.1	54.0	72.2
GL58	61.7923	−49.3872	9	345.8	70.0	318.4	69.5	1.2	1778.0	66.6	38.3
GL59	61.7939	−49.3805	9	348.2	59.4	330.9	61.1	4.1	161.1	63.9	5.5
GL60^{BC}	61.7905	−49.4057	12	354.8	66.3	343.4	67.5	2.6	282.4	75.4	356.8
GL61	61.7901	−49.4096	9	322.9	78.2	302.5	76.2	2.5	415.3	64.5	70.7
GL62	61.7843	−49.3867	8	318.9	59.5	352.2	57.5	3.3	285.5	65.9	325.7
GL63	61.8233	−49.2737	9	156.6	−65.0	147.1	−66.6	5.7	83.9	67.8	21.0
GL65	61.8341	−49.2625	8	325.9	53.6	339.6	54.0	4.7	139.9	59.8	345.5
GL66	61.9131	−49.3689	8	300.0	67.1	316.7	69.1	2.0	741.4	65.4	38.5
GL67	61.9260	−49.3669	11	123.9	−55.9	138.6	−59.9	2.7	280.0	57.5	19.5
GL68	61.9356	−49.5565	8	317.8	60.2	309.4	59.2	8.9	39.4	52.7	28.4
GL69	61.9305	−49.5887	9	348.2	69.7	334.6	71.2	3.4	237.1	75.6	26.5
GL70	61.9284	−49.6056	8	309.5	67.2	326.4	68.0	4.3	164.4	68.9	25.0
GL71	61.9335	−49.6280	9	290.7	78.2	9.1	78.2	1.2	1809.5	84.5	142.8
GL73	62.0167	−49.6874	6	312.9	67.4	324.9	68.8	4.4	229.0	68.9	28.7
GL74	62.0186	−49.6787	9	343.7	63.0	4.4	59.0	2.1	599.9	67.6	301.4
GL75	62.1105	−49.6055	10	323.6	45.9	333.6	44.4	5.4	81.4	49.9	348.7
GL76	62.1108	−49.6003	9	320.1	58.3	335.8	56.9	5.2	97.4	61.2	352.9
GL77$^{Ar/Ar.\ 140.2}$	62.2709	−49.5817	9	138.4	−66.1	171.7	−64.7	2.2	536.2	73.6	331.0
GL79	62.2476	−49.7716	9	336.4	47.1	331.0	47.4	3.3	244.6	51.3	353.2
GL80	62.7038	−50.3530	9	350.5	52.8	350.5	52.8	3.0	293.3	60.1	325.7
GL81$^{Rb-Sr.\ 149.2}$	62.658	−50.2782	9	312.0	47.2	322.9	50.2	5.0	108.0	50.4	4.0
GL82	62.7087	−50.4042	7	139.9	−63.6	150.0	−64.5	1.9	979.4	66.5	9.6
*GL84 + 83$^{Ar/Ar.136.5}$	62.8155	−50.3927	11	133.1	−42.6	153.1	−45.6	3.3	193	50.1	348.5
Mean N			29	325.7	65.3	335.2	65.3	4.1	43.9	71.3	6.5
										A_{95} = 5.8	K = 22.3
Mean R			11	142.7	−58.9	153.0	−60.1	5.5	69.1	63.9	2.1
										A_{95} = 7.0	K = 43.9
Mean N + R			**40**							**69.3**	**5.0**
										A_{95} = 4.6	**K = 25.1**

Notes: Lat and Long – sampling sites coordinates; N – number of samples used to calculate site mean paleomagnetic directions; D_g (D_s) and I_g (I_s) are the calculated paleomagnetic declination and inclination in geographic (stratigraphic) coordinates; α_{95} and k are the 95% confidence circle and the concentration parameter for paleomagnetic directions (Fisher, 1953); P_{lat} and P_{long}, latitude and longitude of virtual geomagnetic poles (VGPs); A_{95} and K are the 95% confidence circle and the concentration parameter for VGP distribution. N and R indicate normal and reversed polarity of the site (group) mean paleomagnetic directions, respectively. * - combined data from paleomagnetic sites tested with fold tests (see text). $^{Ar/Ar,\ Rb-Sr.\ Age,}$ next to the site ID indicate the geochronology method and the nominal age, obtained from a particular dyke in this study and in Larsen et al. (1999; 2009).

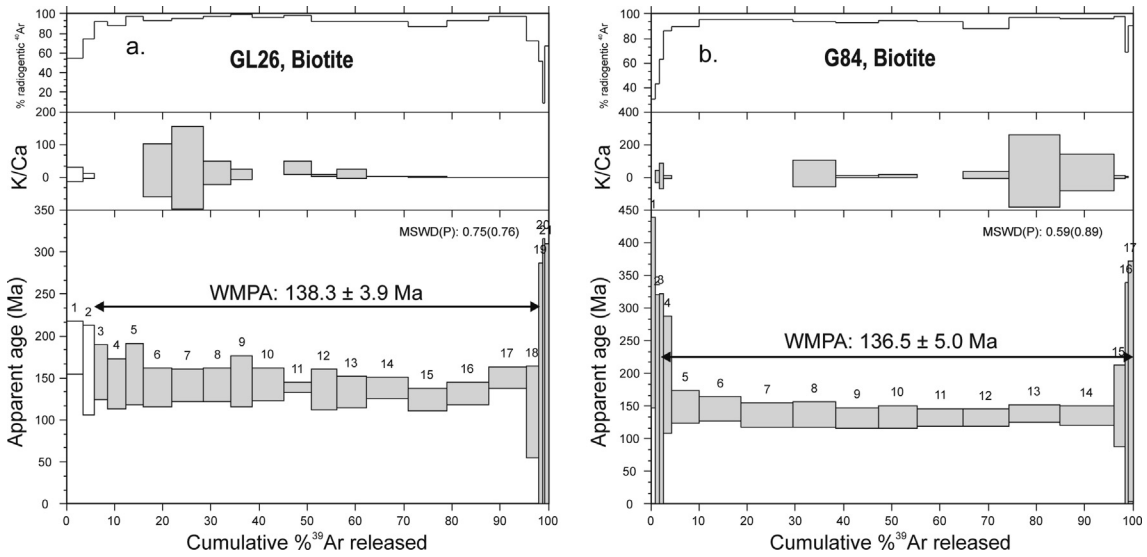

Fig. 3. The results of $^{40}Ar/^{39}Ar$ incremental heating experiments (degassing spectra) on biotite crystals from two samples from two Greenland dykes; **(a),** sample GL26; **(b)**, sample GL84.

ples from the baked host-rock revealed a magnetization direction indistinguishable from that measured from the dyke (Fig. 7 a, b and e; 7f, g and j), indicating a thermally induced magnetic overprint. This overprint component decreases and eventually disappears with increasing distance from the dyke, indicating positive baked contact tests (Fig. 7 c, d and 7h, i).

Three dykes were sampled twice at different localities, characterized by varying dip angles and directions. In order to test whether our data require correction for the structural tilt, paleomagnetic directions obtained from these dykes were subjected to a series of fold tests. The samples' directions showed better grouping after tilt correction (Fig. 8). A substantial increase in Fisher (1953) precision parameter (Fig. 8 a, c; Table 3) for two dykes (sites GL46-49 and GL83-84) suggests a pre-tilting age of the magnetic remanence. A subtle dip-angle difference of 5° between the two localities for the third dyke (sites GL45-50), resulted in a less prominent but yet noticeable improvement of the samples' directions clustering (Fig. 8 f, Table 3). The Watson and Enkin (1993) and the direction-correction (Enkin, 2003) fold tests gave very consistent results, indicating that the best grouping of paleomagnetic directions is achieved at 126 ± 45.3%, 116.8 ± 35.3%, and 99.5 ± 87.6% of untilting for dykes GL46-49, GL83-84, and GL45-50, respectively. Rather large 95% confidence intervals for the test results are exclusively due to small differences between dip angles and directions at two sampling locations. We also tested these data with the fold test of McFadden and Jones (1981), which utilizes a different approach: instead of probing the clustering of paleomagnetic direction as a function of untilting degree, it tests the hypothesis of whether the tilt-corrected directions for the two fold limbs can be considered as drawn from the same distribution of directions. Data from dykes GL46-49 and GL83-84 pass the fold test, whereas those from dyke GL45-50 were characterized by indeterminate test results owing to the small difference in the dyke's dip angle and direction between the two sampling sites. Overall, the results of the fold tests imply that the dykes suffered minor tilting from initially vertical dips after acquiring their magnetic remanence. Accordingly, we used the tilt-corrected site-mean directions for our paleomagnetic analyses. Paleomagnetic data from dykes sampled at two separate locations were combined to calculate a single mean direction for each individual dyke (independent cooling unit).

Twenty-nine of the 40 accepted sites yielded normal polarity ChRM directions with the Fisher (1953) mean D = 335.2°, I = 65.3° (α_{95} = 4.1, k = 43.9). Eleven site means form an antipodal reversed polarity group of directions with a group-mean D = 153.0°, I = −60.1° (α_{95} = 5.5°, k = 69.1) (Table 3, Fig. 9). The mean directions for the two polarity groups pass the reversal test of McFadden and McElhinny (1990) with classification *B* and associated angle between the means γ = 5.3° (critical angle between the means γ_{cr} = 7.4°). The corresponding Fisher means for virtual geomagnetic poles (south VGPs), calculated from the accepted normal and reversed site means are located at P_{lat} = 71.3° S, P_{long} = 6.5 °E (A_{95} = 5.8, K = 22.3, N = 29) and P_{lat} = 63.9° S, P_{long} = 2.1° E (A_{95} = 7.0°, K = 43.9, N = 11), respectively. Consistent with the mean paleomagnetic directions, the mean VGPs are not significantly different and pass the reversal test of McFadden and McElhinny (1990) with classification *B* (angle between the means γ = 7.5° and critical angle γ_{cr} = 12.2°). A paleomagnetic pole, computed from all 40 VGPs has the following coordinates and associated Fisher (1953) statistics: P_{lat} = 69.3° S, P_{long} = 5.0° E, A_{95} = 4.6°, K = 25.1 (Table 3).

In order to test whether paleosecular variations were properly sampled by our data set, we calculated the angular dispersion of the virtual geomagnetic poles using the equation:

$$S^2 = \frac{1}{N-1}\sum_{i=1}^{N}\Delta_i^2$$

where N is the number of individual VGPs and Δ_i is the angle between the i-th VGP and the mean pole (Cox, 1970). The *S*-value was corrected for within-site dispersion (S_w) related to intrinsic variation within a lava flow and experimental uncertainty using:

$$S_b^2 = S^2 - \frac{1}{N}\sum_{i=1}^{N}\frac{S_{wi}^2}{n_i}$$

where S_{wi} represents the within-site dispersion associated with the i-th site, and n_i is the number of paleomagnetic sample directions used to compute the corresponding site-mean direction and the VGP (McFadden et al., 1991). The calculated angular dispersion S_b = 15.9 ± 6.3° is indistinguishable from the 14 ± 2° S_b value predicted by the Late Jurassic – Early Cretaceous PSV model of Doubrovine et al. (2018) at a latitude of 45° (the paleolatitude calculated from the mean paleomagnetic inclination). The agreement suggests that our paleomagnetic data adequately sample PSV and the new pole faithfully represents the time-averaged geomagnetic

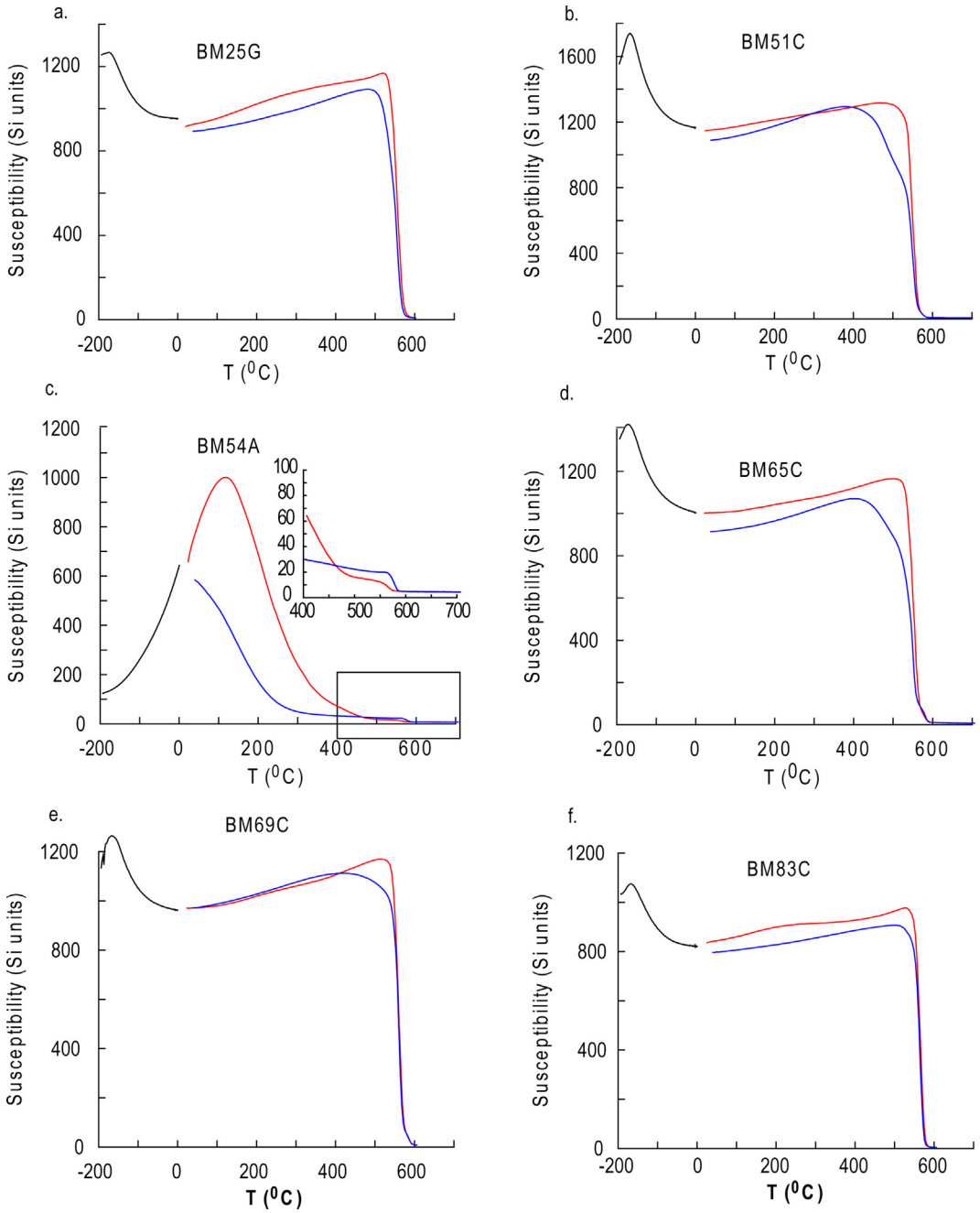

Fig. 4. Typical dependence of low-field magnetic susceptibility (κ) versus temperature measured from the Greenland dyke samples showing heating (red curves), cooling (blue curves), and low-temperature cycles (black curves); (**Inset in c**), the high-temperature (400–700 °C) part of heating and cooling cycles, showing κ(T) irreversibility associated with formation of a magnetic phase with ~580–585 °C Curie temperature, likely magnetite.

field. Our new Greenland pole merits the highest scores $Q = 7$ and $R = 7$ on the classical and updated paleomagnetic data quality and reliability scales of Van der Voo (1990) and Meert et al. (2020), respectively.

4. Discussion

4.1. Magnetization age and pole position

Our new $^{40}Ar/^{39}Ar$ results agree well with available geochronological data (Table 2). We note, however, that the previously reported $^{40}Ar/^{39}Ar$ ages were calculated using the decay constants of Steiger and Jäger (1977). For consistency, we recalculated those ages using updated parameters (Renne et al., 2010). Corrected data are within analytical error of the original ages, yet shifted towards slightly older ages (Table 2). Overall, available geochronology data show a spectrum of ages, which suggests that the studied dykes were emplaced during a protracted episode of intrusive magmatism between 150 Ma (Late Jurassic) and 140–135 Ma (Early Cretaceous). It should be noted that the oldest dykes of aillikite/alnöite and monchiquite composition are dated by U/Pb (150.5 ± 1.5 Ma, N = 3, calculated as the weighted mean of all U-Pb ages listed in Table 2) and Rb/Sr (149.5 ± 2.2 Ma, N = 3, calculated as the weighted mean of all Rb-Sr ages listed in Table 2), respectively.

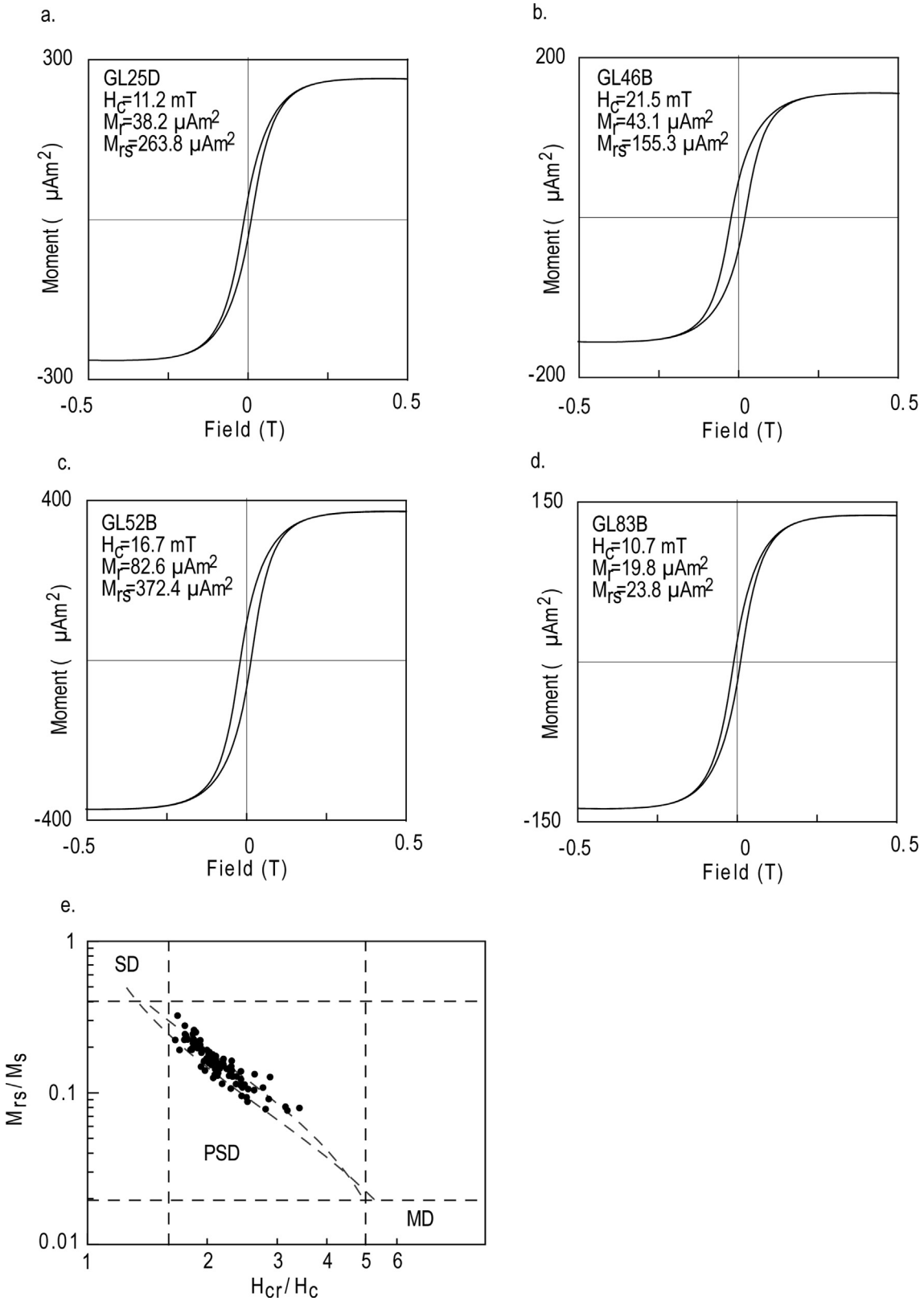

Fig. 5. Magnetic hysteresis properties measured from the Greenland dykes. **(a–d)**, Typical magnetic hysteresis loops after paramagnetic slope correction. **(e)**, Day plot (Day et al., 1977). Abbreviations are the following: SD, single domain; PSD, pseudo-single domain; MD, multidomain; M_{rs} and; M_s are saturation remanent and saturation magnetic moments, respectively; H_c, coercivity field; H_{cr}, coercivity of remanence. Gray dashed lines show SD-MD mixture models from Dunlop (2002).

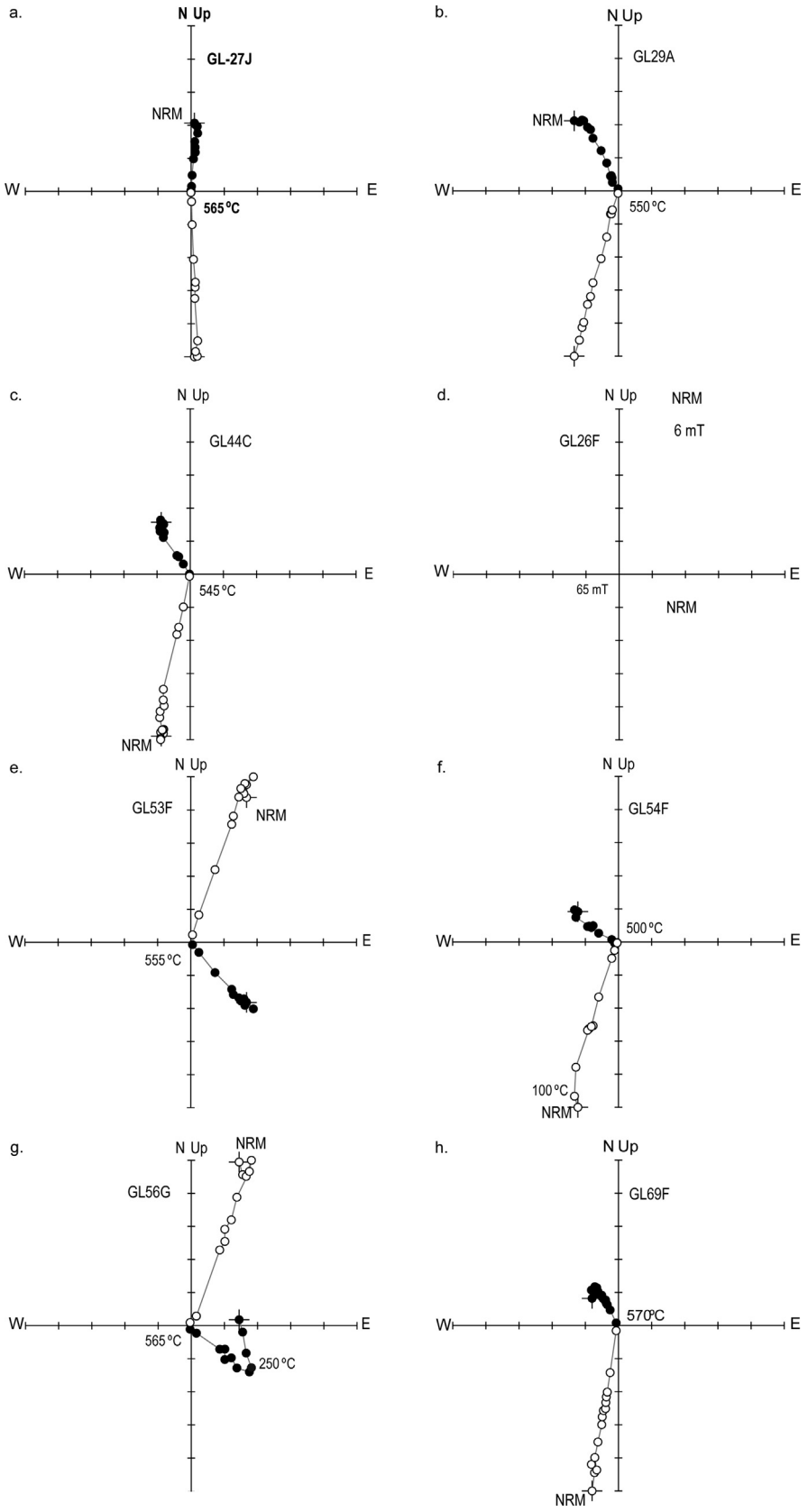

Fig. 6. Examples of vector endpoint diagrams for the Greenland dykes (open symbols are data-point projections on a vertical plane; solid symbols are projections on a horizontal plane).

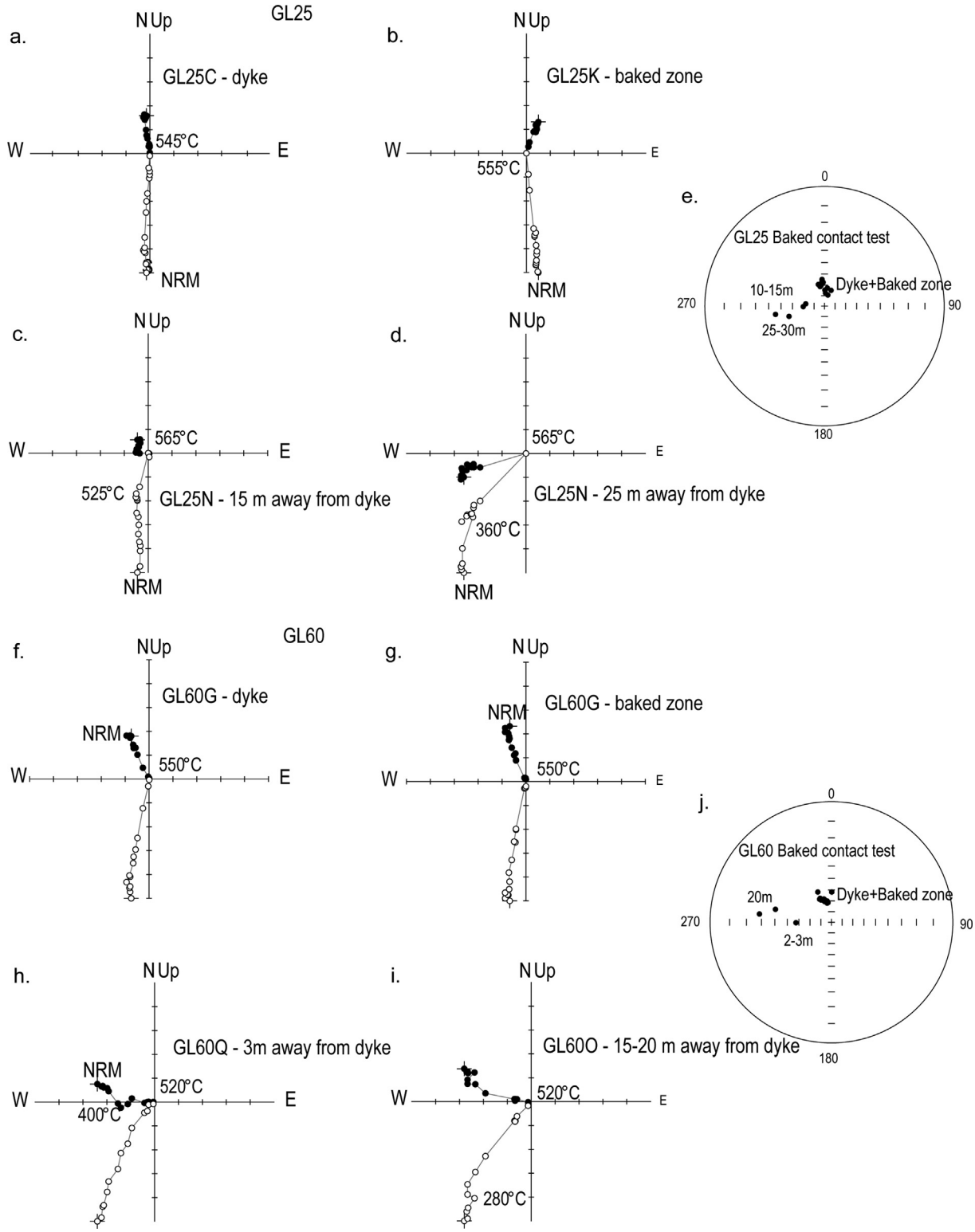

Fig. 7. Two **e**xamples of positive baked contact tests for the Greenland dykes (sites GL 26 and GL 84). **(a)** and **(f)**, Vector endpoint diagrams (VED) showing individual sample directions; **(b)** and **(g)**, VEDs showing directions from baked zones for sites GL25 and GL 60, respectively; **(c, d)** and **(h, i)**, VEDs showing individual sample directions measured from the samples collected from progressively increasing distances from the dykes; **(e)** and **(j)** – equal-area projections showing directions of the dykes, baked zones and country rock. The decrease of unblocking temperatures of the secondary thermal overprint in the country rocks as a function of distance from the contact with dykes is generally consistent with the thermal aureole models (e.g. Annen, 2017).

Conversely, the youngest dykes of mafic (basaltic) composition are exclusively dated with $^{40}Ar/^{39}Ar$ (138.2 ± 2.7 Ma, N = 5; weighted mean of all $^{40}Ar/^{39}Ar$ ages in Table 2). At face value, this suggests a 12 Myr difference between the various dyke phases, but it is well known that the $^{40}Ar/^{39}Ar$ system is much more mobile than the U/Pb system. In rocks that have been extensively dated with both methods (e.g., the Parana-Etendeka large igneous province; Owen-Smith et al., 2019), the $^{40}Ar/^{39}Ar$ ages are systematically younger

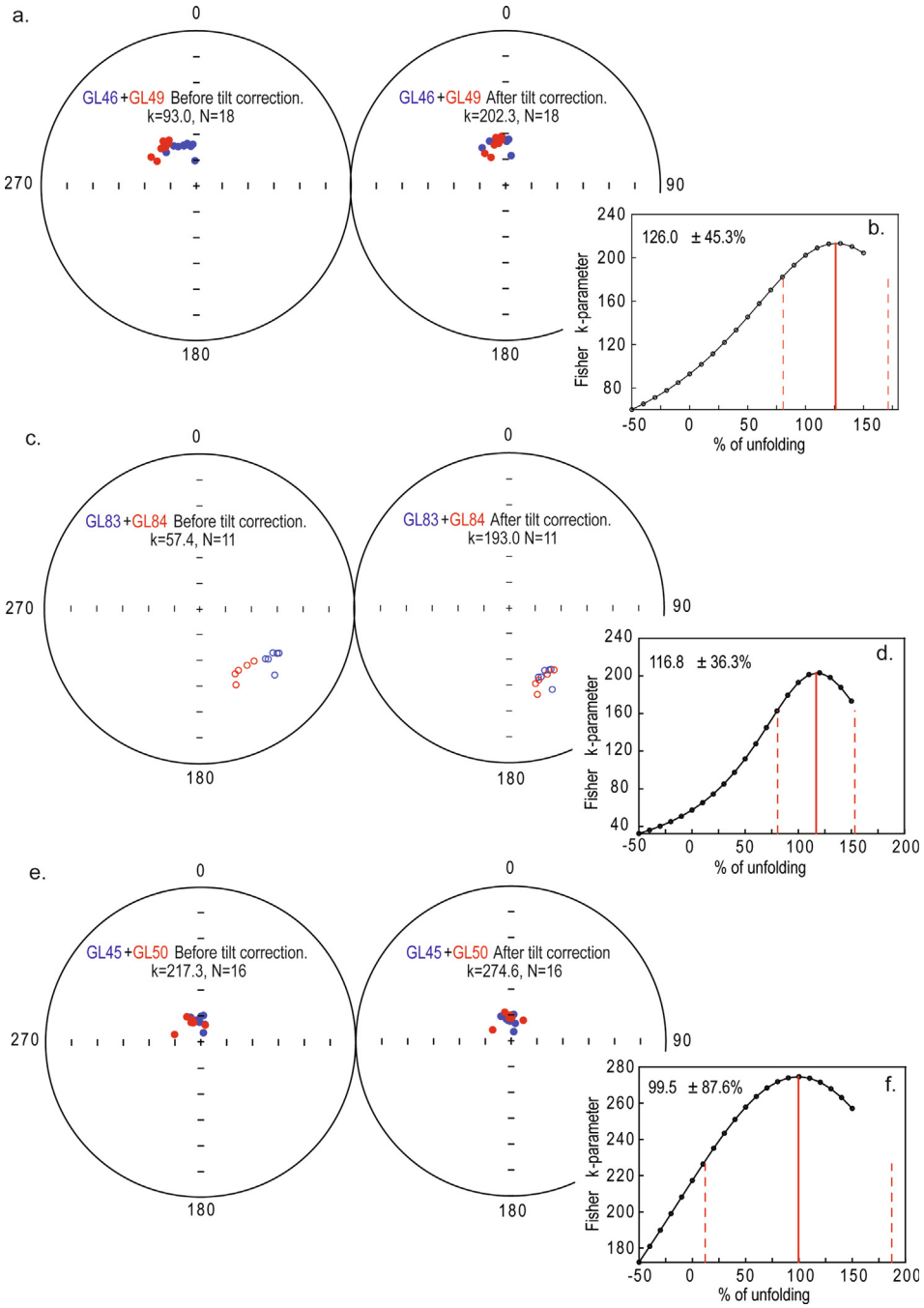

Fig. 8. Results of the fold test for three dykes. **(a, c and e)**, Equal-area projections showing paleomagnetic directions of individual samples before and after the correction for structural tilt. **(b, d and f),** Results of the Watson and Enkin (1993) fold test showing the Fisher (1953) precision parameter *k* as a function of untilting degree. Solid and dashed red lines correspond to the maximum-*k* degree of untilting and 95% confidence interval bounds, respectively.

than those measured with the U-Pb method. The actual difference in age may therefore be less than 12 Myr. While the available dates suggest that the magmatic activity has spanned several millions of years, the special distribution of dated dikes does not show distinct locations corresponding to the Late Jurassic and Early Cretaceous ages (Fig. 2). The 136.5 ± 3.9 Ma dyke (this study, site GL84) is located several kilometers from the 149.2 ± 2.7 (paleomagnetic site GL81), 156.0 ± 14, and 152.1 ± 1.6 Ma dykes (Larsen et al., 2009). The 149.8 ± 0.6 Ma dyke is located about 17 km to the east from the 140.2 ± 1.4 Ma dyke (Fig. 2). Interestingly, all $^{40}Ar/^{39}Ar$-dated dykes (136.5 ± 4.9 to 140.2 ± 1.4 Ma), which can be directly linked to our sampling sites, are of reversed polarity whereas one dyke dated to 149.2 ± 2.7 Ma (Rb-Sr) is normally magnetized (Fig. 9b). Yet statistically, normal and reverse mean directions are not distinguishable from being antipodal, based on the reversal test.

The site-mean paleomagnetic directions obtained from dykes representing all ages form a well-clustered group (after flipping the reversed polarity directions by 180°). Fig. 9c and 9d show the data quantiles for the site-mean declination and inclination plotted against the uniform and exponential quantiles expected for a Fisher distribution. The formal tests for the conformity of declination data with a uniform distribution and inclination data with an exponential distribution (Fisher et al., 1987) yielded values of M_u (uniform) and M_e (exponential) statistics below the critical values

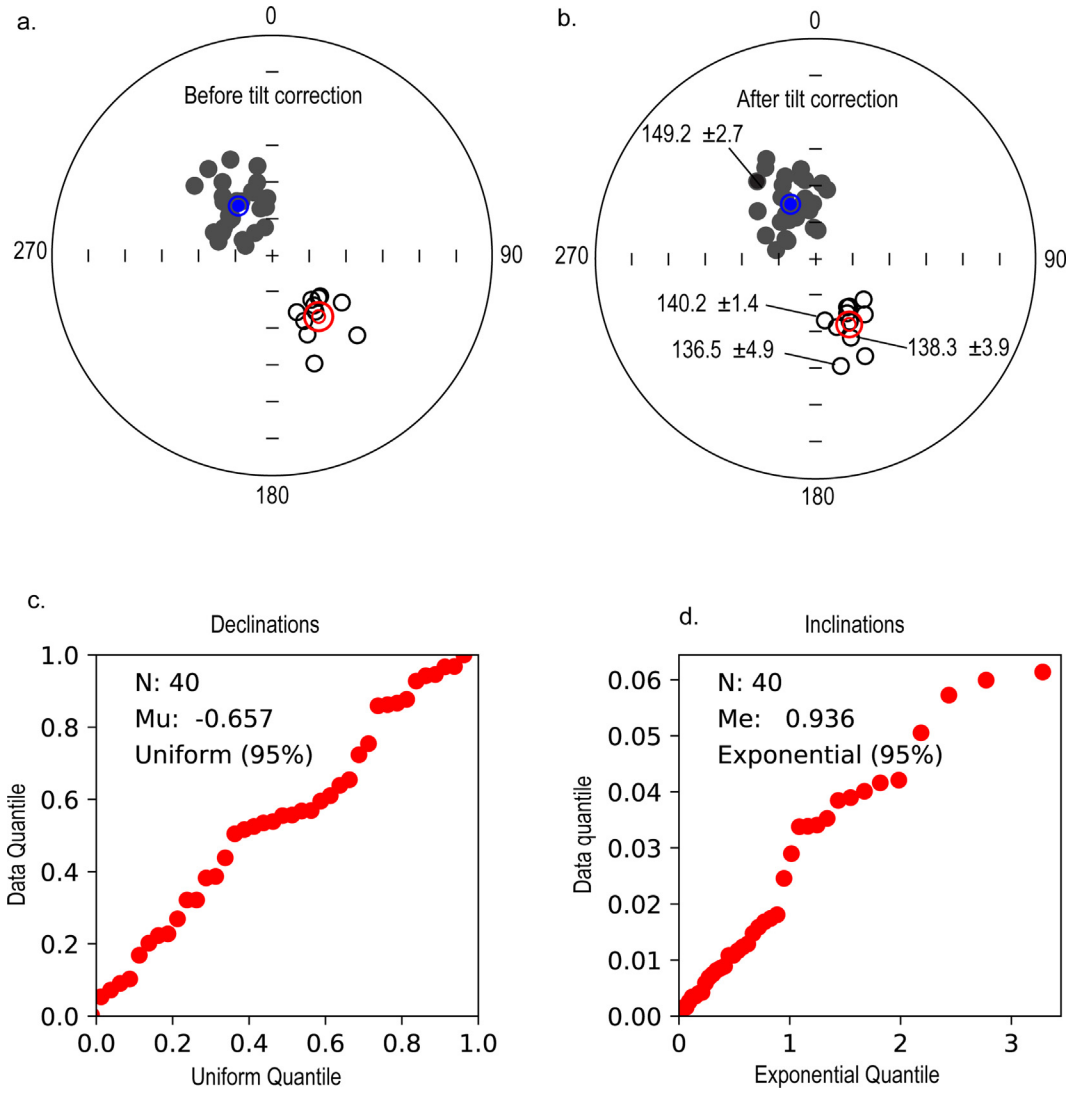

Fig. 9. Paleomagnetic results from the Greenland dykes. Equal-area projections show the accepted paleomagnetic site-mean normal (filled circles) and reversed (open circles) polarity directions and their group-mean direction with the 95% confidence circle (α_{95}) (blue and red for normal and reversed polarity directions, respectively). **(a),** Before and **(b),** after correction for structural tilt; the results of quantile–quantile test for paleomagnetic declinations **(c)** and inclinations **(d),** plotted against the uniform and exponential quantiles expected for a Fisher distribution (Fisher, 1987). The test was performed on the tilt-corrected paleomagnetic directions using Tauxe et al. (2016) PmagPy package for paleomagnetic data processing.

corresponding to the 5% significance level, indicating that the distribution of directions is consistent with the Fisherian model. In addition to the positive reversal test, a Fisherian distribution of paleomagnetic directions suggests a rather stable geomagnetic field and insignificant polar motion (despite different dyke ages), and multiple positive baked contact tests clearly indicate primary thermoremanent magnetizations acquired during the initial cooling of the dykes. We assign the new paleomagnetic pole a nominal mean age of 147.6 ± 3.4 Ma (2σ), which was calculated as a weighted average of all available age determinations (N = 11, Table 2), where statistical weights were proportional to the inverse of the analytical variance.

The new Greenland paleomagnetic pole is located at P_{lat} = 73.9° S, P_{long} = 0.4° E, A_{95} = 4.6° after rotation to North American coordinates using the rotation parameters of Torsvik et al. (2012) (Euler pole coordinates E_{lat} = 67.5°N, E_{long} = 118.5°W, and the rotation angle E_{ang} = −14°). In North American coordinates, the pole (Fig. 10 a) plots close to the ~156 Ma mean VGP from the Ontario kimberlites (Kent et al., 2015), and mid-way along the proposed monster polar-shift track. Our new Greenland pole (Fig. 10 a) statistically overlaps with that reported in Piper (1975) (P_{lat} = 76.2° S, P_{long} = 9.9° E; North American coordinates), but is very different from the pole of Fahrig and Freda (1975) (P_{lat} = 61.3° S, P_{long} = 336.7° E; North American coordinates). The new Greenland pole is statistically different from the ~145 Ma mean pole of Kent and Irving (2010) and appears incompatible with the rapid Late Jurassic monster polar shift, as argued below.

4.2. Jurassic APWP and the proposed monster polar shift

The proposed Jurassic monster polar shift comprises ~31° of polar motion between ~160 Ma (after the 190–160 Ma standstill) and ~145 Ma (Kent and Irving, 2010; Kent et al., 2015; Muttoni and Kent, 2019) at an average rate of 2.1°/Myr. This rate is close to the upper limit of theoretical estimates for TPW (Tsai and Stevenson, 2007; Steinberger and Torsvik, 2010). Torsvik et al. (2012, 2014) have identified two TPW phases between 200 and 140 Ma. Both phases are characterized by a clockwise rotation

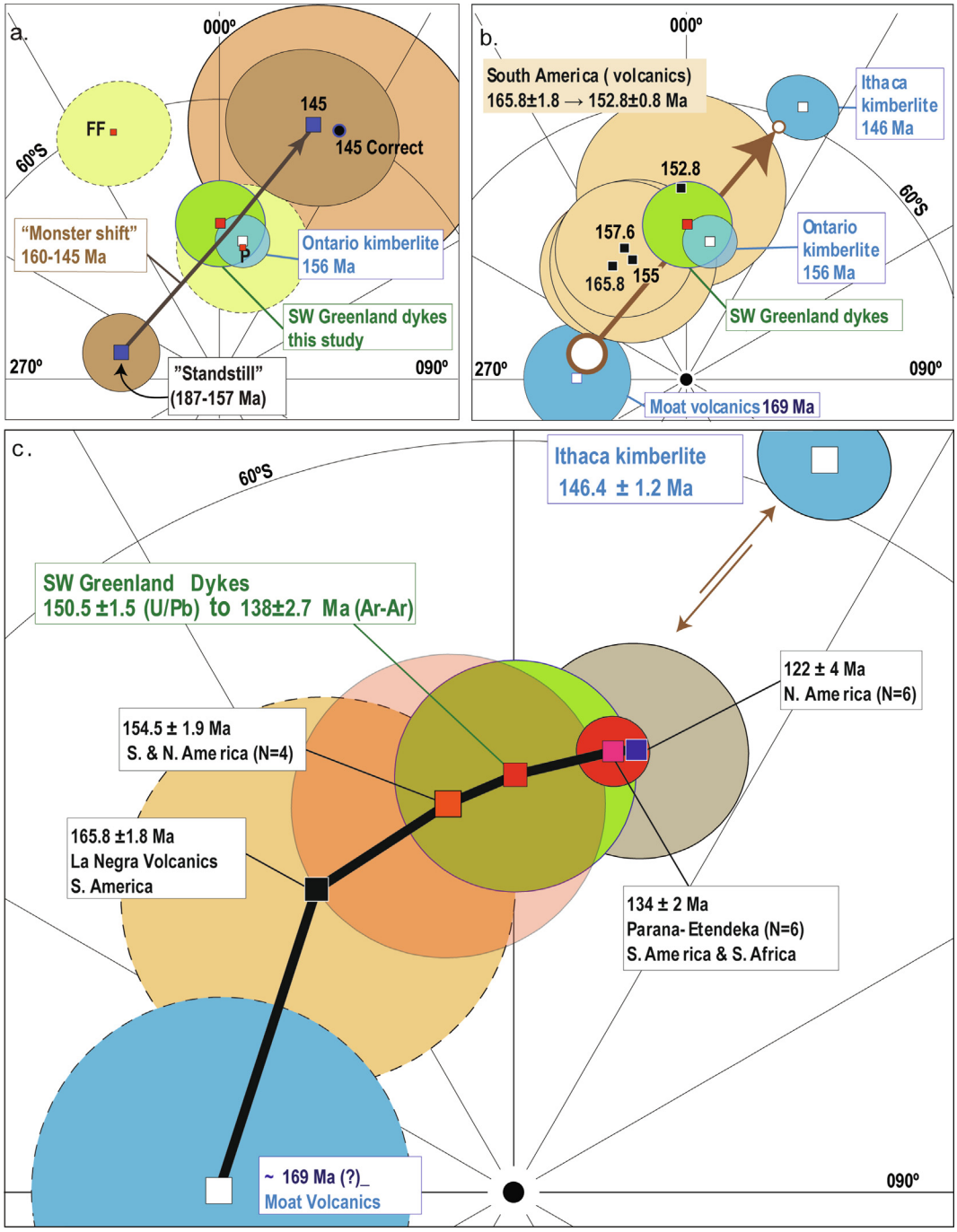

Fig. 10. The Jurassic monster polar shift assessment. (a) The Jurassic monster polar shift between 160 and 145 Ma (beginning and tip of the large, brown arrow in all panels; poles #1 and #5 in Table 1) shown together with our new Greenland pole (#6 in Table 1), the mean Ontario kimberlite pole (#3), the mean 145 Ma pole, calculated using the original three poles (Hinlopenstretet dolerites, Ithaca kimberlite and the "erroneous" location of the Swartuggen-Bumbeni pole). The "145 Correct" pole with large A_{95} corresponds to the recalculated using the corrected Swartuggen-Bumbeni pole mean 145 Ma pole (see text). FF and P are paleomagnetic poles from SW Greenland dykes reported by Fahrig and Freda (1975) and Piper (1975), respectively. (b), The Jurassic monster shift compared with some recent poles derived from volcanic rocks in South America (see text and Table 1), Ithaca kimberlite pole (#4), Moat volcanics pole (#2), and Ontario kimberlite pole (#3). (c), The The 154-122 Ma apparent polar wander path constructed using the new Greenland paleomagnetic pole, mean poles from North and South Americas, and South Africa (see text and Table 1); The 146 Ma Ithaca Kimberlite pole is shown to illustrate the discrepancy between this pole and the new 147.6 Ma high-quality Greenland pole. All paleopoles are shown with their 95% confidence ovals (A_{95}). All poles are shown in orthogonal south polar projections.

around an equatorial axis (Fig. 1d) with a combined 41° of polar wander, but with much slower rates (0.8°/Myr between 150 and 140 Ma and 0.45°/Myr between 200 and 150 Ma). While all these studies consistently indicate a TPW episode during the Late Jurassic to Early Cretaceous, TPW magnitudes, rates, and timing differ significantly between different studies. These notable differences require thorough scrutiny.

The so-called 190–160 Ma polar standstill defined by Kent and Irving (2010) included poles with ages between 187 and 157 Ma (Fig. 1 b, ## 42-53 in *table 5* of Kent and Irving, 2010), with the

two youngest poles (167 and 157 Ma, ## 43 and 42 in *table 5* of Kent and Irving, 2010) from South America. However, the most recent studies of 166–153 Ma volcanic rocks in South America (Fu et al., 2020; Cervantes-Solano et al., 2020; Gonzales et al., 2019) yield paleomagnetic poles that, when reconstructed to the North American reference frame, are distributed along the Jurassic monster polar shift segment with the youngest poles located close to our new Greenland pole and the 156 Ontario kimberlite pole (Table 1, Fig. 10b). Although the recently published South American paleomagnetic poles have relatively large A_{95} circles and are not statistically different from each other, the 165.8 ± 1.8 and 157.6 ± 3 Ma poles differ significantly from the mean standstill paleomagnetic pole (Fig. 10 a, b, Table 1), indicating at least some polar wander during the youngest portion of the 187–157 Ma interval. The youngest North American pole belonging to the polar standstill is the ~169 Ma Moat volcanics (Fig. 10 b, Table 1), but the age of the Moat volcanics is uncertain, with Rb/Sr dates suggesting an age between 175 and 168 Ma) while U/Pb dating indicating an older age by approximately 10 Myr (Town et al., 2019). The younger limit of the Jurassic monster polar shift in North America is represented by the 146.4 ± 1.2 Ma Ithaca kimberlite pole of Van Fossen and Kent (1993) (Fig. 10 b, Table 1). In addition to the Ithaca kimberlite pole, the younger limit of the Jurassic monster polar shift is defined by two other paleomagnetic poles (Fig. 11 a, Table 1), namely the Hinlopenstretet pole from Svalbard (Halvorsen, 1989) and the Swartuggen-Bumbeni pole from South Africa (Hargraves, 1989; Hargraves et al., 1997). The Late Jurassic – Early Cretaceous sedimentary poles from Adria (Channell et al., 2010; Muttoni et al., 2013), when corrected for potential inclination flattening and rotated to the North American reference frame (Muttoni and Kent, 2019), were used to corroborate the vast and rapid Late Jurassic polar wander (Fig. 11b). Unfortunately, several problems with the aforementioned paleomagnetic data appear to weaken these arguments and overall interpretations. In the following sections we discuss these problematic paleomagnetic data in detail.

4.2.1. Hinlopenstretet paleomagnetic pole

K-Ar analyses of the Svalbard mafic intrusions in the 1960s and 1970s yielded two groups of plagioclase ages of ~110 and 144 Ma (Gayer et al., 1966; Burov et al., 1977). The older age was interpreted as potentially reflecting the emplacement of the rocks and the Hinlopenstretet paleomagnetic pole (Halvorsen, 1989) was therefore originally assigned an age of 144 Ma. The robustness of these K-Ar ages, however, has recently been questioned. The geochronology study of Nejbert et al. (2011) reported 39 K-Ar age determinations obtained from samples of Svalbard dolerites, including 23 samples from the eastern Svalbard dolerite belt. With the exception of one 257.0 ± 7.3 Ma age, all reported determinations indicate 125 Ma and younger ages for the Svalbard intrusive rocks. No ages close to 144 Ma have been reported. The results of this study agree with recent U-Pb (Corfu et al., 2013) and $^{40}Ar/^{39}Ar$ (Polteau et al., 2016) ages measured from samples of western and central Svalbard dolerites. The updated geochronology of the Svalbard dolerites indicates that magmatic activity on Svalbard was confined to a short time interval between approximately 125 and 120 Ma. Therefore, the Hinlopenstretet paleomagnetic pole (Fig. 11a) is significantly younger than previously thought. Accordingly, we assign an age of 122 Ma for this pole and exclude it from the calculation of the reference pole position at ~145 Ma. Note also that the 122 Ma Hinlopenstretet pole is somewhat anomalous as it does not match very well-defined 122 Ma poles from North America (Supplementary material figure S1).

4.2.2. Swartuggen-Bumbeni paleomagnetic pole

Originally calculated at P_{lat} = 31.7°S, Pl_{ong} = 104.3°E, A_{95} = 6.3° by Hargraves et al. (1997), the Swartuggen-Bumbeni pole averages paleomagnetic data from the ~145 Ma Bumbeni syenite (four site-mean directions) and two coeval Swartuggen kimberlite fissures, located ~550 km from Bumbeni. Kent and Irving (2010) transferred this pole to the North American coordinates using rotation parameters from Roest et al. (1992), but used erroneous coordinates: P_{lat} = 31.7°S, P_{long} = 94.3°E (note the 10° difference in longitude), which resulted in the rotated position listed in Table 1 and shown in Fig. 11a with the dashed 95% confidence ellipse and labelled "Erroneous".

The erroneous Swartuggen-Bumbeni pole has appeared in a series of studies and has been repeatedly used to advocate for the Jurassic monster polar shift (e.g. Kent et al., 2015; Muttoni and Kent, 2019; Fu et al., 2020). Furthermore, we were not able to reproduce the exact Swartuggen-Bumbeni pole location of Kent and Irving (2010) using the rotation parameters they specified, regardless of the use of initially reported or more westerly pole coordinates. Notwithstanding this, the correct Swartuggen-Bumbeni pole location in the North American reference frame, transferred using rotation parameters of Torsvik et al. (2012), is located at P_{lat} = 57.6°S, P_{long} = 46.9° E (Table1, Fig. 11a), i.e. about 10° away from the position reported by Kent and Irving (2010). The great-circle distance between the corrected Swartuggen-Bumbeni pole and the Ithaca kimberlite pole is 12.6° and their 95% confidence circles do not overlap, indicating that the two poles are clearly inconsistent. In fact, the Swartuggen-Bumbeni pole is truly anomalous among Mesozoic Gondwana poles and has not been included in most published APWPs (e.g., Torsvik et al., 2008, 2012; Besse and Courtillot, 2002).

In addition, the age for the Swartuggen-Bumbeni pole is not well defined. While K-Ar and $^{40}Ar/^{39}Ar$ whole-rock analyses of Bumbeni syenite yielded ages of 140–145 Ma (Burger and Coertze, 1973, Allsopp et al., 1984), Rb-Sr isotope compositions (Allsopp et al., 1981) indicate a ~10 Myr younger age of 133 ± 5 Ma for the same rocks. Bristow and Cleverly (1983) considered the Rb-Sr isochron age to be more reliable than the K-Ar and $^{40}Ar/^{39}Ar$ ages, which likely reflect excess argon due to weathering and/or sample processing, thus yielding an erroneously old age. With this in mind, and considering the revision of the pole position, we conclude that the Swartuggen-Bumbeni pole cannot be used as an appropriate reference pole for constraining the Jurassic APWP.

4.2.3. Ithaca kimberlite pole

In contrast to the Swartuggen kimberlites and the Bumbeni syenite, the emplacement age of the Ithaca dykes was robustly determined at ~146 Ma by U-Pb dating of perovskite (Kent et al., 2015). The Ithaca paleomagnetic pole (Figs. 10, 11) is based on seven site-mean paleomagnetic directions of both polarities that pass the reversal test, but have very low angular dispersion (3.5°, Van Fossen and Kent, 1993). Six out of seven dykes yielded normal polarity NRM directions. The reversed polarity magnetization has been isolated from six samples representing a single dyke and symmetry between normal and reversed directions may thus be fortuitous. The authors, however, interpreted the low angular dispersion of paleomagnetic directions as due to *some process* in the kimberlite dykes that caused the prolonged acquisition of chemical remanent magnetization (CRM) in addition to primary TRM. They argued that this complex thermochemical remanent magnetization (TCRM) was acquired by the Ithaca dykes over a period of time, which was sufficiently long to average out paleosecular variations. Although it is extremely difficult to discriminate between CRM (or TCRM) and pure TRM (e.g. Dunlop and Özdemir, 1997), prolonged acquisition of TCRM is possible. Yet, the data do not rule out an alternative scenario of accidental symmetry of the normal and reversed polarity mean paleomagnetic directions, which may

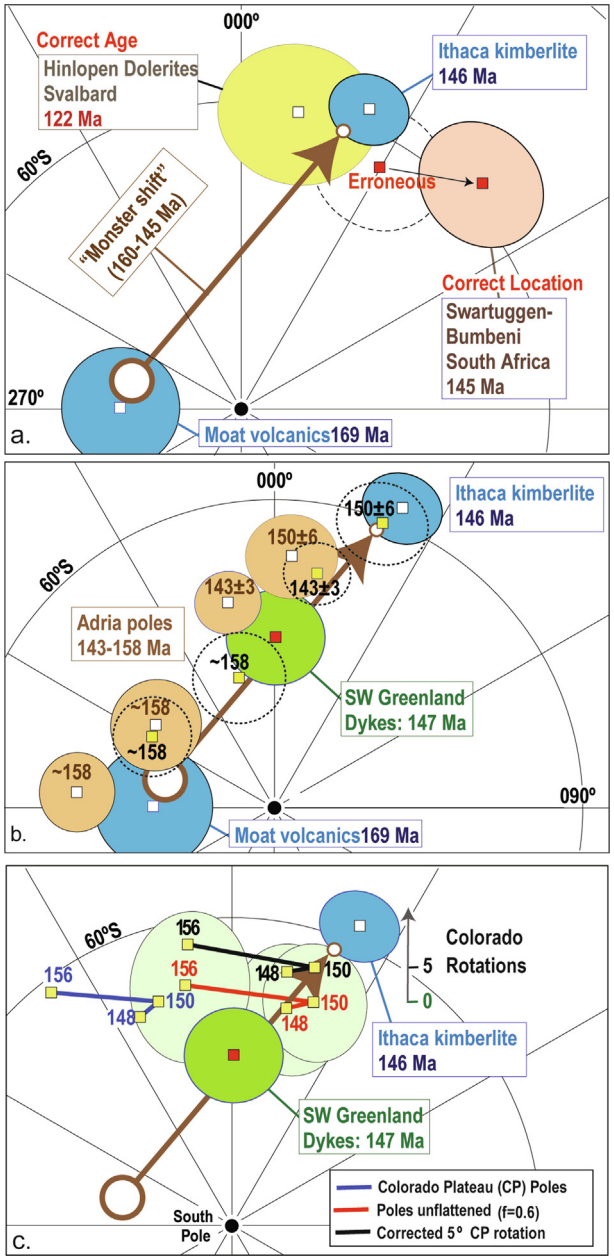

Fig. 11. **(a)** The 160–145 Ma Jurassic monster polar shift (beginning and tip of the large brown arrow in all panels; poles #1 and #5 in Table 1) shown together with the Moat volcanics (#2 in Table 1) and the original three poles (Hinlopenstretet dolerites, Ithaca kimberlite and the "erroneous" location of the Swartuggen-Bumbeni pole) that were used to calculate the 145 Ma mean pole. **(b)** The Jurassic monster shift also compared with the Adria poles (see text), corrected according to Van Hinsbergen et al. (2020) and Torsvik et al. (2012) (poles with light-brown shaded A_{95}s) and Adria poles from Muttoni and Kent (2019) (with A_{95}s shown as dashed ovals). **(c)** The Jurassic monster shift compared with the late Jurassic sedimentary poles from the Colorado Plateau, with and without correction for inclination shallowing ($f = 0.6$). Poles connected with the black line are corrected for a possible 5° rotation of the Plateau relative to stable North America (see text). In all panels, the paleomagnetic (south) poles are shown in North American coordinates (Table 1). All paleopoles are shown with their 95% confidence ovals (A_{95}) except the Colorado Poles that are shown with dp/dm ovals (only for inclination flattening-corrected poles). All poles are shown in orthogonal south-polar projections.

in fact may represent two instantaneous readings of the geomagnetic field.

A natural question arises at this point – was the TCRM acquisition sufficiently long lasting to average PSV by individual Ithaca kimberlite dykes? The dykes are characterized by a high degree of serpentinization (Van Fossen and Kent, 1993), a process associated with heat release and growth of secondary minerals, including magnetite, therefore causing acquisition of chemical remanent magnetization. The duration of serpentinization largely depends on a number of physical and chemical properties of the rock, including the size of intrusions, porosity, permeability, and initial olivine content (e.g. Afanasyev et al., 2014). A mathematical model (Afanasyev et al., 2014) has shown that depending on olivine fraction in the kimberlite matrix, a cone-shaped intrusion (with a near-surface width of 540 m) undergoes complete serpentinization during a time interval of ~380 to 2000 years, which is generally not sufficient to average out PSV (McElhinny and McFadden, 2000). Laboratory oxidation of synthetic olivine over a course of several days (Hoye and Evans, 1975) resulted in crystallization of magnetite capable of acquiring and retaining a stable CRM, further indicating that magnetite crystallization associated with olivine alteration is a relatively rapid process. Given the width of the Ithaca dykes, ranging from several centimeters to few meters (Van Fossen and Kent, 1993), we suspect that paleomagnetic directions measured from the Ithaca dykes may not represent the time-averaged geomagnetic field.

Additional concerns regarding the Ithaca kimberlite pole emerge from a somewhat ambiguous baked contact test for one of the Ithaca dykes. The thermal remanent magnetization component, acquired by the host limestone during emplacement of the dyke, has a mean paleomagnetic direction 14° shallower and statistically different from that obtained from the dyke (Van Fossen and Kent, 1993). The authors interpreted this difference as due to an incomplete removal of the present-day viscous magnetization. Alternatively, the difference between the mean paleomagnetic directions could result from different timing of acquisition of thermal and chemical remanence by the host rock and dyke, respectively.

In Fig. 10c we have averaged three South American poles (152.8–157.6 Ma; Fig. 10b, Table 1) and the Ontario kimberlite (156 Ma) pole in North America to obtain a 154.5 Ma mean pole (Table 1). We also show a mean 134 Ma pole from the Parana-Etendeka large igneous province and a well-defined 122 Ma mean pole from North America. Apparent polar wander between 154.5 and 122 Ma amounts to only 7.5° (great-circle distance) or 0.2°/Ma, which is due to the fact that North America/Greenland did not move much in latitude and was dominated by westward drift from about 140 Ma. Our new Greenland pole plots in an expected location between the 154.5 and 134 Ma mean poles (Fig. 10c), but a nominal age of 147.6 ± 3.4 Ma, overlapping with the age of the Ithaca kimberlite (146.2 ± 1.2 Ma), is obviously problematic because the poles are 18° apart. The only way to reconcile the Ithaca pole is to (i) consider that the Greenland dykes may range in age by as much as 12 Myr, i.e. 150 Ma for oldest dykes (dated by U/Pb) and 138 Ma for the youngest mafic dykes (dated by Ar-Ar), and (ii) that the Ithaca kimberlite was emplaced between the two dyke phases. This requires that the TPW monster shift has to be redefined to have occurred after 150 Ma followed by counter-clockwise TPW of about the same amount sometime between 146 and 138 Ma. This scenario requires TPW rates between ~4.5 and 2.5°/Myr that exceed the limit of theoretical estimates for TPW (e.g. Tsai and Stevenson, 2007) and therefore appears unlikely. Overall, several issues, including possibly under-sampled paleosecular variation, potentially delayed acquisition of chemical remanence or a combination of the two, may challenge the robustness of the Ithaca kimberlite paleomagnetic pole.

In summary, the 145 Ma point that defined the younger end of the monster polar shift proposed in the original study of Kent and Irving (2010) is based on three paleomagnetic poles, one of which (Hinlopenstretet) has been shown to correspond to a more than 20

Myr younger age, and another (Swartugen-Bumbeni) that was erroneously reconstructed and is also likely to be some 10 million years younger than its nominal age of 145 Ma. The remaining ~146 Ma pole from seven Ithaca kimberlite dykes that have an unclear history of magnetization may also be prone to bias arising from incomplete averaging of PSV. Hence, the 145 Ma pole of Kent and Irving (2010) may not be as robust as claimed, and we now turn to the discussion of paleomagnetic data from Adria and their place in the story of the Jurassic APWP controversy.

4.2.4. Paleomagnetic data from Adria

Muttoni and Kent (2019) have recently presented support for the Jurassic monster polar shift based on an analysis of paleomagnetic data from Adria. Rotated from African to North American coordinates, the Jurassic – Early Cretaceous paleomagnetic poles from Adrian sedimentary rocks reveal a large amount of polar wander, which is apparently consistent with the vast and rapid Jurassic polar motion (Fig. 11b). However, the validity of this argument relies on the assumption of perfect rigidity and stability of Adria and its tectonic coherence with Africa.

Based on the observation that paleomagnetic data from Adria are not consistent with those from Europe but perhaps better fit coeval data from Africa, Muttoni et al. (2013) argued that Adria represents a stable and tectonically coherent promontory of Africa, and all relative motions between Adria and Africa have been negligibly small and unresolvable with paleomagnetism. Yet, the tectonic coherence between Adria and Africa is not supported by geologic constraints. The presence of Miocene rifts along the margin of Northern Africa and deformational structures within central Adria (e.g., Le Breton et al., 2017) are at odds with the idea of a perfectly stable Adria. Complicating the picture even further is a 9.8 ± 9.5° post-Eocene counterclockwise rotation (Van Hinsbergen et al., 2014) and up to 5 mm/year of present-day northward motion (Van Hinsbergen et al., 2020) of Adria relative to Africa. It is also worth mentioning that some Adria poles used to substantiate tectonic stability of Adria and the Jurassic monster polar shift, namely those measured from the Torre de'Busi and Colle de Sogno sequences (Muttoni et al., 2005; Channell et al., 2010), were corrected for 10° clockwise vertical axis rotation with respect to the rest of Adria data in order to match the coeval African paleomagnetic poles (Channell et al., 2010), which indicates that in addition to the motion of Adria relative to the neighboring blocks, local rotations/motions within Adria took place.

Kent and Muttoni (2020) argued for a perfect stability of Adria with respect to NW Africa based on the similarity of 280 Ma mean Adria and Gondwana poles. The latter pole was calculated using five individual paleomagnetic poles, three of which are either younger (273 Ma pole from Morocco trachyandesite, Daly and Pozzi, 1976) or can well be significantly older (286 ± 6 Ma poles from Australia; Clark and Lackie, 2003) than 280 Ma. The 280.5 Ma pole from Morocco volcanics of Westphal et al. (1979) was also included in the average, but has a large uncertainty (A_{95} = 20.9°) and hence cannot be considered reliable. The new 280 Ma paleomagnetic pole obtained from the Morocco volcanics (Domeier et al., 2021) is statistically different and located 8.3° from the mean Adria pole of Kent and Muttoni (2020). We also note that the new pole of Domeier et al. (2021) is similar to the mean 280 Ma Gondwana pole of Torsvik et al. (2012). The position of the mean Adria pole with respect to the Morocco pole (Domeier et al., 2021) and the mean Gondwana pole (Torsvik et al., 2012) is consistent with counterclockwise rotation of Adria relative to the NW Africa. We further note that the mean Gondwana pole of Kent and Muttoni (2020) does not contain any data from sedimentary rocks, which were excluded as unreliable due to potential problems caused by sedimentary inclination shallowing. Interestingly, all post-280 Ma paleomagnetic data from Adria were obtained from sedimentary rocks, which are not immune to inclination shallowing problems.

Muttoni and Kent (2019) corrected Adrian data for both inclination shallowing and local rotations, and then rotated the Adria poles to the North American coordinates assuming that Adria was rigidly locked to North Africa. They argued that the location of the 150 ± 6 Ma mean pole close to the 146 Ma Ithaca kimberlite pole

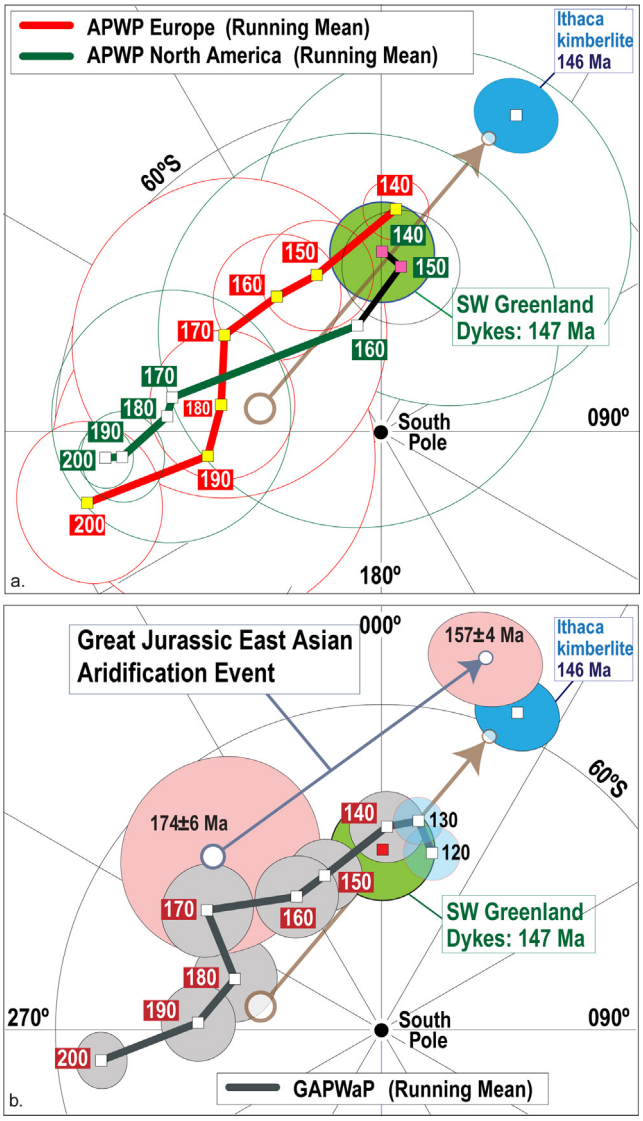

Fig. 12. Apparent polar wander paths (APWPs). **(a),** The APWPs for Europe and North America (excluding all poles from the Colorado Plateau). Running-mean path with 20 Myr sliding window, updated from Torsvik et al. (2012) and shown together with the new Greenland pole. Because Torsvik et al. (2012) included Late Jurassic poles from Colorado (corrected for inclination shallowing; Fig. 10d) the North American mean poles for 140 and 150 Ma were smoothed and plotted very differently (see Fig. 1a), and in fact much closer to the European APWP. For the North American APWP, the Ithaca kimberlite pole is substituted with our new Greenland pole (rotated to the North American frame). **(b),** The global APWP (GAPWaP) from 200 to 120 Ma, updated from Torsvik et al. (2012), including new poles reported from South America (Fig. 10b), new Parana-Etendeka poles (Table 1), and our new Greenland pole. Note that neither the Jurassic monster polar shift nor the Great Jurassic East Asian Aridification event (East Asia displaced southward and out of the northern wet belt; Figs. 1, 13) are compatible with the updated APWPs (see text). In addition, the two TPW episodes, namely the 160-145 monster polar shift (Kent and Irving, 2010) and the 174-157 Ma (Yi et al., 2019) contradict each other with regard to their timing. A major part of the 174-157 Ma event was proposed to occur during the so-called polar standstill, which predated the 165-145 Ma monster polar shift of Kent and Irving (2010).

(Fig. 11b, stippled pole) supports the hypothesis of the monster shift. As an exercise, we repeated their procedure but corrected for relative rotations between Adria and North East Africa as deduced from the model of Van Hinsbergen et al. (2020; see their supplementary GPlates project and rotation file), and then rotated the poles to the North American frame according to Torsvik et al. (2012). By doing so, we observed that the 150 ± 6 and 143 ± 3 Ma Adria mean poles (Fig. 11 b, poles with shaded ovals) actually reconstruct closer to our 147.6 Ma Greenland pole than to the Ithaca kimberlite pole. Conversely, two poles of approximately 158 Ma in age plot near the 190–160 Ma standstill mean pole (the large, white open circle defining the start of the monster shift in Fig. 11b), but their locations are clearly to the west of the global distribution of volcanic poles between 158 and 153 Ma (Fig. 10b). Overall, given the uncertain tectonic history of Adria, with respect to the neighboring blocks, as well as potential issues related to inclination shallowing and local tectonic rotations, we advise that extra caution should be exercised when adopting paleomagnetic poles from Adria into the construction of global APW paths.

4.2.5. Colorado Plateau paleomagnetic poles

Paleomagnetic data from the Colorado Plateau have also been used to address Jurassic polar wander. As an example, Kent and Irving (2010) corrected paleomagnetic data from the lower (~156 Ma) and upper (150–148 Ma) Morrison Formations (Fig. 11c) for sedimentary inclination shallowing (using a correction factor f = 0.55) and assuming a 13° clockwise rotation of the Colorado Plateau relative to North America. They argued that the adjusted upper Morison poles plot close to the 146 Ma Ithaca kimberlite pole, lending additional support for the vast and rapid polar wander during the Late Jurassic. We have repeated this exercise using a more conservative and widely used inclination shallowing correction factor of f = 0.6 and show that the Colorado poles fall near our new Greenland pole (Fig. 11c). We also show that a more modest 5° rotation of the Plateau (e.g. Bryan and Gordon, 1986, 1990) brings the upper Morison Formation poles closer to the Ithaca kimberlite pole, indicating that the monster polar shift can equally be supported or rejected, depending on the magnitude of tectonic rotation chosen to correct the data.

While the exact amount of the Colorado Plateau rotation relative to cratonic North America remains unclear and may range between ≤5° and 13° (see Steiner, 2003 for review), the major problem with Colorado Plateau paleomagnetic data stems from the nature of natural remanence residing in these rocks. In a recent study, Muttoni and Kent (2019) resampled the Late Jurassic Morrison formation and argued that the poles from both the lower and upper Morrison formations have been variably overprinted during the Cretaceous and thus cannot be used for APW determination. Given the uncertainty around the Jurassic poles from the Colorado Plateau (the likely presence of secondary remanence overprints) and the largely unconstrained magnitude of Colorado Plateau rotations versus stable North America (estimated from palaeomagnetic data) we have excluded all Colorado Plateau poles from our APWPs that we derive below.

5. Revised Jurassic-Early Cretaceous (200–140 Ma) APWPs

APWPs conveniently summarize paleomagnetic data for continents or tectonic blocks, and they are commonly constructed with the use of spherical splines or applying the running-mean method. With the latter technique, the location on the APWP corresponding to a specific age is calculated as a Fisherian mean (Fisher, 1953) of paleomagnetic poles whose ages fall within a selected time window (e.g., 20 Myr) centered on that age. Pole uncertainty is expressed as a circle of 95% confidence (A_{95}) and estimated for each mean pole using Fisherian statistics. Both the spline and running-mean techniques average out random biases of individual paleomagnetic poles and smooth the APWPs. Here, we present updated APWPs for North America and Europe as well the global APWP for the Jurassic - Early Cretaceous (Supplementary Data, Table S2). A more extensive scrutiny of paleomagnetic data for the entire Phanerozoic is currently underway.

If we exclude all poles from the Colorado Plateau and substitute the 146 Ma Ithaca kimberlite pole with our new 147 Ma Greenland pole (rotated to the North American frame), the European and North American APWPs become grossly similar (Fig. 12a, Table 4), and the average great-circle distance between individual poles of

Table 4
Running Mean Apparent polar wander paths (APWPs) for North America, Europe, and the global APWP, shown in Fig. 12. Notes: P_{lat} and P_{long}, latitude and longitude of virtual geomagnetic poles (VGPs) in North American coordinates; A_{95} is the radius of 95% confidence circle. N indicates the number of paleomagnetic poles, averaged to calculate the mean pole.

APWPs	Age (Ma)	N	A_{95} (°)	P_{lat} (°N)	P_{lon} (°E)	Figure
Europe	200 ± 10	5	7.2	−62.4	256.3	12a
	190 ± 10	3	14.9	−74.4	262.0	12a
	180 ± 10	3	6.6	−75.6	279.5	12a
	170 ± 10	3	14.4	−73.6	301.7	12a
	160 ± 10	6	5.7	−74.8	322.3	12a
	150 ± 10	6	5	−74.9	337.7	12a
	140 ± 10	1	2.9	−70.0	3.8	12a
North America	200 ± 10	16	2.7	−64.9	264.6	12a
	190 ± 10	11	4	−66.5	264.4	12a
	180 ± 10	3	11.2	−70.8	274.1	12a
	170 ± 10	2	35.5	−71.1	279.3	12a
	160 ± 10	3	17.9	−80.4	347.4	12a
	150 ± 10	3	5.2	−75.2	6.8	12a
	140 ± 10	1	4.6	−73.9	0.4	12a
GAPWaP	200 ± 10	37	2.5	−64.4	263.7	12b
	190 ± 10	37	3.4	−73.7	272.2	12b
	180 ± 10	30	3.8	−76.2	289.2	12b
	170 ± 10	15	4.2	−71.1	304.5	12b
	160 ± 10	16	3.7	−76.0	327.6	12b
	150 ± 10	15	3.3	−75.4	340.0	12b
	140 ± 10	13	3.3	−71.8	1.5	12b
	130 ± 10	13	3.3	−71.8	1.5	12b
	120 ± 10	24	2.2	−71.0	10.0	12b

the same age is 6.3 ± 1.7°. That is a significant improvement over the original APWPs of Torsvik et al. (2012; here shown in Fig. 1a) where the great-circle distance between the North America and European APWPs averaged 9.4 ± 3.9°. If we pool together paleopoles globally, we notice that the GAPWaP (Fig. 12b, Table 4) is grossly similar to the European and North American paths (Fig. 12a, Table 4), the location of the Greenland pole fits perfectly with the GAPWaP whilst the coeval Ithaca pole is a clear outlier.

In contrast to the questionable and possibly biased paleomagnetic poles from North America, South Africa, and Adria, the new Greenland pole derived from high-quality paleomagnetic data does not support the Jurassic monster polar shift. Instead, it indicates a relatively steady polar motion during the Jurassic, and overall, the revised GAPWaP (Table 4, Fig. 12b) dictates APW rates of ~0.7 ± 0.2°/Myr and a total amount of APW of ~41° between 200 and 140 Ma. In addition, the so-called monster polar shift associated with clockwise TPW between 160 and 145 Ma (brown arrow in Fig. 12b), for which we do not find sufficiently strong evidence, would also require a rapid phase of counterclockwise TPW to reach the 130 and 120 Ma mean poles (Fig. 12b), which are based on multiple high-quality volcanic poles from around the world, including North America (e.g. McEnroe, 1996a,b, Table 1). Our results do not support such TPW countermotion and instead suggest much slower and gradual temporal APWP progression, compatible with paleomagnetic data on a global scale.

Yi et al. (2019) invoked an episode of Jurassic TPW that rapidly drove the East Asian Blocks (EAB) southward (exemplified by North China in Fig. 13a) to explain the Great Jurassic East Asian aridification event. However, this event supposedly occurred between 174 and 157 Ma (Yi et al., 2019) and *not* between 160 Ma and 145 Ma as in the model of Kent et al. (2015). The TPW episode proposed by Yi et al. (2019) is based on two volcanic paleopoles from North China. The older paleopole (174 ± 6 Ma) places North China at much higher latitudes than all existing plate models, with the northern margin of the EAB (the Central Mongolian belt of Amuria) overlapping with Eurasia. This paleogeography implies that the Mongol-Okhotsk Ocean (Fig. 13 a, b) must have closed before 174 Ma (Yi and Meert, 2020), and not in the Early Cretaceous, as suggested by others (e.g., Van der Voo et al., 2015; Torsvik and Cocks, 2017). Yi and Meert (2020) argued that following the early to middle-Jurassic closure of the Mongol-Okhotsk Ocean the EAB became an integral part of Eurasia, but if paleomagnetic data of Yi et al. (2019) are taken at face value, they suggest that the ocean basin has reopened by ~157 Ma and finally closed in Early Cretaceous time (Fig. 13b). We consider that the tectonic coherence of the EAB with Eurasia since the Middle Jurassic is unlikely, but if we accept the model of Yi and Meert (2020), we can simply reconstruct the North China poles to the North American reference frame (Fig. 12b) using relative plate circuits for Europe-North America. Doing so, we observe that the reconstructed 174 Ma pole overlaps with our mean 170 Ma GAPWaP pole, whereas the location of the 157 Ma pole is highly anomalous and inconsistent with any of the coeval poles used in the construction of the GAPWaP (Tables 1 and 4). We note that new paleomagnetic data from North China (Fig. 13b; Z1-Z3) reported in Zhang et al. (2020) do not support the fast TPW model of Yi et al. (2019) and seriously question the high latitude of North China at 174 ± 6 Ma (Fig. 13b, NC1) with its implication for a closed Mongol-Okhotsk Ocean at that time (Fig. 13a, North China and Amuria blue shaded and labelled NC_1 and A_1).

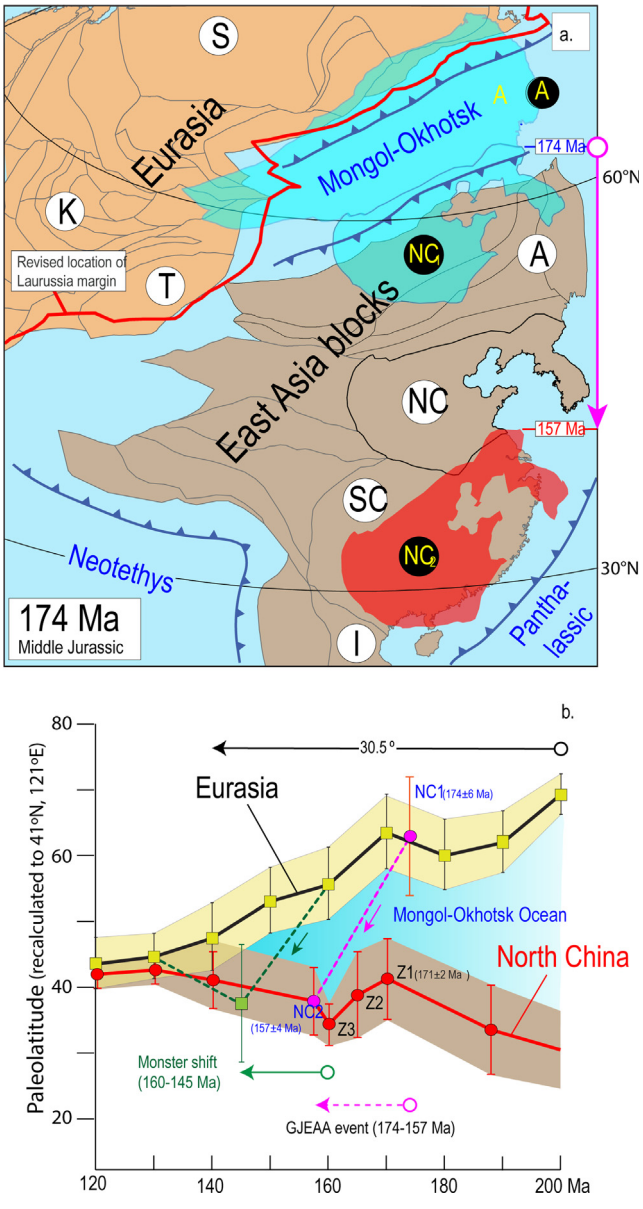

Fig. 13. (a) Plate reconstruction of the Eurasian margin (Torsvik and Cocks, 2017) and the East Asian Block (EAB) at 174 Ma. Our refined location of the Eurasian margin (based on GAPWaP in Fig. 12b, Table 3) is shown as a thick, red line. The much higher latitude location of North China (NC) and Amuria (A) at 174 ± 6 Ma (Yi et al., 2019), which must apply to the entire EAB, is shown in blue transparent shading (NC_1 and A_1) and implies that the Mongol-Okhotsk Ocean was closed by the Early Jurassic and not during the Early Cretaceous (Van der Voo et al., 2015). We have also superimposed the location of North China at 157 Ma (NC_2) according to Yi et al. (2019); the dramatic southerly change in latitude of about ~25° between 174 and 157 Ma (see panel b: Y1 and Y2) was interpreted as TPW and must then apply to the entire planet for which there is no sufficient evidence. Other abbreviations: I, Indo China; K, Kazakhstan terranes; SC, South China; T, Tarim; S, Siberia. Orthogonal projection centered on 45°N and 120°E. **(b),** Paleolatitudes for Eurasia (based on GAPWaP in Fig. 12b but recalculated to Eurasia frame) shown with a yellow-shaded confidence envelope. Eurasian and North China (Zhang et al. 2020) latitudes are recalculated to a common reference location (41°N, 121°E). NC1 and NC2 estimates based on the poles reported in Yi et al. (2019) and the large latitude differences were used to argue for the Great Jurassic East Asia Aridification (GJEAA) event, explained by fast clockwise true polar wander (TPW) between 174 ± 6 and 157 ± 4 Ma. New poles and latitude estimates Z1-Z3 by Zhang et al. (2020) challenge the reliability of the NC1 pole, which age-wise overlaps with Z1 (171 ± 2 Ma). The analysis of Zhang et al. (2020) agrees well with the reconstruction of Van der Voo et al. (2015) with regard to Mongol-Okhotsk Ocean closure in the Early Cretaceous, but contradicts the reconstruction in panel a (Yi et al., 2019). Torsvik et al. (2014) estimated slow clockwise TPW (30.5o around an axis located at 0oN and 11oE) between 200 and 140 Ma. The monster shift model and the GJEAA event (Yi et al. 2019) are both explained by fast TPW, but the timing is very different and the two models contradict each other. As an example, the monster shift model invokes a polar standstill between 190 and 160 Ma, i.e. during the 174–157 Ma TPW event of Yi et al. (2019). Both the monster shift and the 174–157 Ma TPW event are questioned in this study (see text).

Two paleomagnetic poles from North China with overlapping ages of 174 ± 6 Ma (Yi et al., 2019) and 171 ± 2 Ma (Zhang et al. 2020) yield paleolatitudes that differ by ~22° (Fig. 13b), emphasizing that claims of extremely rapid TPW based on a 'pole-by-pole' comparison should be treated cautiously. There are several paleomagnetic poles that are indeed anomalous and left unexplained in the literature, probably not due to TPW but perhaps as a consequence of various paleomagnetic pitfalls. These include rock and magnetic age uncertainties, time averaging and recording issues, inadequate demagnetization procedures in the laboratory, unaccounted tectonic corrections or local magnetic declinations, as well as technical glitches such as erroneous vector transformations from drilling co-ordinates to geographic co-ordinates, which are rarely admitted in the literature (e.g. Eneroth, 2006). We conclude that both contrasting models for fast clockwise Jurassic TPW, the 160–145 Ma monster shift of Kent and Irving (2010) and the episode invoked by Yi et al. (2019), appear unlikely upon careful global analysis of available paleomagnetic data.

6. Summary and conclusions

We report the results of a new, integrated paleomagnetic and ^{40}-Ar/^{39}Ar geochronology study of Late Jurassic – Early Cretaceous coast-parallel mafic dykes of southwest Greenland. Paleomagnetic samples from 40 dykes yielded well-defined characteristic remanent magnetization components of both polarities. A primary nature of the characteristic remanence was verified by four positive baked contact tests and the presence of paleomagnetic directions of both polarities that pass the reversal test. The available and newly reported geochronology data indicate that the dykes may have been emplaced over a protracted period, perhaps in two main phases separated by several Myrs, but did not record any substantial polar wander. The new Greenland pole has a nominal age of 147.6 ± 3.4 Ma and yields the highest possible paleomagnetic data quality score Q = 7 (Van der Voo, 1990), as well as the maximum score R = 7 on the recently proposed data-reliability scale of Meert et al. (2020). Notwithstanding the age uncertainty, the new, high-quality pole is in conflict with the Kent and Irving (2010) model invoking fast Jurassic monster polar shift. Instead, the new pole, as well as an updated global APWP, indicate steady polar motion with rates of ~0.7°/Myr, which is two to three times slower than the rates inferred from a few selected paleomagnetic poles supporting the rapid polar shift. Our critical reappraisal of the Jurassic monster polar shift suggests that it is an artifact due to deficiencies in paleomagnetic and geochronology data, which were previously used to argue for its existence. The new paleomagnetic pole plots close to the coeval paleomagnetic poles from Europe and effectively closes the Jurassic-Cretaceous gap between the Laurentian and European APWPs.

CRediT authorship contribution statement

Evgeniy V. Kulakov: Conceptualization, Investigation, Writing - original draft, Data curation. **Trond H. Torsvik:** Conceptualization, Writing - original draft, Writing - review & editing. **Pavel V. Doubrovine:** Writing - review & editing. **Trond Slagstad:** Investigation, Writing - review & editing. **Morgan Ganerød:** Investigation, Writing - review & editing. **Petter Silkoset:** Investigation. **Stephanie C. Werner:** Investigation, Writing - review & editing.

Declaration of Competing Interest

The authors declare that they have no known competing financial interests or personal relationships that could have appeared to influence the work reported in this paper.

Acknowledgements

All data used in our analyses have been generated in the Ivar Giæver Geomagnetic Laboratory at the University of Oslo and are available at www.earthdynamics.org/Greenland/PalmagData.zip. We thank the Research Council of Norway (RCN) for support through its Centers of Excellence funding scheme (project 223272: CEED) and RCN project 274085 for field-work funding. T.S. and M.G. thank the Geological Survey of Norway (NGU) for support. We also thank the Government of Greenland Ministry of Mineral Resources and the Mineral License and Safety Authority for their help and assistance in obtaining all necessary permits and licenses.

Appendix A. Supplementary data

Supplementary data to this article can be found online at https://doi.org/10.1016/j.gr.2021.05.021.

References

Afanasyev, A.A., Melnik, O., Porrit, L., Schumacher, J.C., Sparks, R.S.J., 2014. Hydrothermal alteration of kimberlite by convective flows of external water. Contrib. Mineral. Petrol. 168, 1038. https://doi.org/10.1007/s00410-014-1038-y.

Allsopp, H.L., Bristow, W., Manton, W., Cleverly, R.W., 1981. Rb-Sr geochronology of the Lebombo volcanics. S. African Geodyn. Symp. Proc. Abstracts, 1–2.

Allsopp, H.L.J., Bristow, W., Logan, C.T., Eales, H.V., Erlank, J., 1984. Rb-Sr geochronology of three Karoo-related intrusive complexes. Geol. Soc. of S. Africa Spec. Publ. 13, 281–287.

Annen, C., 2017. Factors affecting the thickness of thermal aureoles. Front. Earth Sci. 5. https://doi.org/10.3389/feart.2017.00082.

Bazard, D.R., Buttler, R.F., 1994. Paleomagnetism of the Brushy Basin Member of the Morrison Formation: Implications for Jurassic apparent polar wander. J. Geophys. Res. 99, B4. https://doi.org/10.1029/93JB03208.

Besse, J., Courtillot, V., 2002. Apparent and true polar wander and the geometry of the geomagnetic field over the last 200 Myr. J. Geophys. Res. 107 (B11), 2300. https://doi.org/10.1029/2000JB000050.

Bristow, J.W., Cleverly, R.W., 1983. A note on the volcanic stratigraphy and intrusive rocks of the Lebombo monocline and adjacent areas. Transactions Geol. Soc.S. Africa 86, 55–61.

Bryan, P., Gordon, R.G., 1986. Rotation of the Colorado Plateau: an analysis of paleomagnetic data. Tectonics 5, 661–667. https://doi.org/10.1029/TC005i004p00661.

Bryan, P., Gordon, R.G., 1990. Rotation of the Colorado Plateau: An updated analysis of paleomagnetic data. Geophys. Res. Lett. 17, 1501–1504. https://doi.org/10.1029/GL017i010p01501.

Burger, A.J., Coertze, F.J., 1973. Radiometric age measurements on rocks from southern Africa to the end of 1971. Bull. Geol. Soc.of S. Africa 58, 46 pp.

Burov, Yu.P., Krasilscikov, A.A., Firsov L.V., Klubov, B.A., 1977. The age of the Spitsbergen dolerites, Norsk Polarinstitutt Årbok 1975, 101–108.

Cervantes-Solano, M., Goguitchaichvili, A., Sánchez Bettucci, L., Morales-Contreras, J., Gogorza, C., Núñez, P., 2020. An integrated paleomagnetic and multispecimen paleointensity study from the late Jurassic Zapicán dike swarm (Uruguay). J. S. Am. Earth Sci., https://doi.org/10.1016/j.jsames.2020.102815.

Channell, J.E.T., Casellato, C.E., Muttoni, G., Erba, E., 2010. Magnetostratigraphy, nannofossil stratigraphy and apparent polar wander for Adria-Africa in the Jurassic-Cretaceous boundary interval. Palaeogeogr. Palaeoclimatol. Palaeoecol. 293 (1–2), 51–75. https://doi.org/10.1016/j.palaeo.2010.04.030.

Clark, D., Lackie, M., 2003. Palaeomagnetism of the Early Permian Mount Leyshon Intrusive Complex and Tuckers Igneous Complex, North Queensland, Australia. Geophys. J. Int., 153(3), 523-547.

Corfu, F., Polteau, S., Planke, S., Faleide, J.I., Svensen, H., Zayoncheck, A., Stolbov, N., 2013. U-Pb geochronology of Cretaceous magmatism on Svalbard and Franz Josef Land. Barents Sea Large Igneous Province. Geol. Mag. 150, 1127–1135. https://doi.org/10.1017/S0016756813000162.

Courtillot, C., Besse, J., Théveniaut, H., 1994. North American Jurassic Apparent Polar Wander: the answer from other continents? Phys. Earth Planet. Int. 82, 87–104.

Cox, A., 1970. Latitude dependence of the angular dispersion of the geomagnetic field. Geophys. J. R. Astr. Soc 20 (3), 253–269. https://doi.org/10.1111/j.1365-246X.1970.tb06069.x.

Daly, L., Pozzi, J.P., 1976. Resultats paleomagnetiques du Permien inferieur et du Trias Marocain; comparaison avec les Donnees Africaines et Sud Americaines. Earth Planet Sci. Lett. 29, 71–80.

Day, R., Fuller, M., Schmidt, V.A., 1977. Hysteresis properties of titanomagnetites: grain size and compositional dependence. Phys. Earth Planet. Int. 13, 260–267.

Dodd, S.C., MacNiocaill, C., Muxworthy, A.R., 2015. Long duration (> 4 Ma) and steady state volcanic activity in the early Cretaceous Paraná-Etendeka Large

Igneous Province: new palaeomagnetic data from Namibia. Earth Planet. Sci. Lett. 414, 16–29. https://doi.org/10.1016/j.epsl.2015.01.009.
Domeier, M., Font, E., Youbi, N., Davies, J., Nemkin, S., Van der Voo, R., Perrot, M., Benabbou, M., Boumehdi, M.A., Torsvik, T.H., 2021. On the Early Permian shape of Pangea from paleomagnetism at its core. Gondwana Res. 90. https://doi.org/10.1016/j.gr.2020.11.005.
Doubrovine, P.V., Velkolainen, T., Pesonen, L.J., Piispa, E.J., Siim, O., Smirnov, A.V., Kulakov, E.V., Biggin, A.J., 2018. Latitude dependence of geomagnetic paleosecular variation and its relation to the frequency of magnetic reversals: observations from the Cretaceous and Jurassic. Geochem., Geophys. Geosyst. 20, 1240–1279.
Dunlop, D.J., Özdemir, Ö., 1997. Rock magnetism. Fundamentals and frontiers. Cambridge Studies in Magnetism Series. 573 pp. Cambridge University Press.
Dunlop, D.J., 2002. Theory and application of the Day plot (Mrs/Ms versus Hcr/Hc) 1. Theoretical curves and tests using titanomagnetite data. J. Geophys. Res. 107, B3, 2056. https://doi.org/10.1029/2001JB000486.
Eneroth, E., 2006. Erratum: Withdrawal (Precam. Res. (2006) 146 (23-45) DOI: 10.1016/j.precamres.2003.09.014
Enkin, R.J., 2003. The direction-correction tilt test: an all-purpose tilt/fold test for paleomagnetic studies. Earth Planet. Sci. Lett. 212, 151–166.
Ernesto, M., Raposo, M.I., Marques, L.S., Renne, P.R., Diogo, L.A., de Min, A., 1999. Paleomagnetism, geochemistry and 40Ar/39Ar dating of the North-eastern Paraná Magmatic Province: tectonic implications. J. Geodyn. 28, 321–340.
Fahrig, W.F., Freda, G., 1975. Palaeomagnetism of the Mesozoic coast-parallel dolerite dikes of West Greenland. Can. J. Earth Sci. 12, 1244–1248.
Fisher, R.A., 1953. Dispersion on a sphere. Proc. R. Soc. London. Series A 217, 295–305.
Fisher, N.I., Lewis, T., Embleton, B.J.J., 1987. Statistical Analysis of Spherical Data. University Press, Cambridge.
Foster, J., Symons, D.T.A., 1979. Defining a paleomagnetic polarity pattern in the Monteregian intrusives. Can. J. Earth Sci. 16, 1716–1725.
Fu, R.R., Kent, D.V., 2018. Anomalous Late Jurassic motion of the Pacific Plate with implications for true polar wander. Earth Planet. Sci. Lett. 490, 20–30. https://doi.org/10.1016/j.epsl.2018.02.034.
Fu, R.R., Kent, D.V., R.Hemming, S.R., Gutiérrez, P., Crevelinge, J.R., 2020. Testing the occurrence of Late Jurassic true polar wander using the LaNegra volcanics of northern Chile. Earth Planet. Sci. Lett., 529, 115835.
Gayer, R., A., Gee, D.G., Harland, W.B., Miller, J.A., Spall, H.R., Wallis, R.H., Winsnes, T. S. 1966. Radiometric age determinations on rocks from Spitsbergen. Norsk Polarinstitutt, Skrifter 137: 1–39, (1).
González, V.R., Puigdomenech, C.G, Emiliano M.Renda. E.M., Boltshauser, B., Somoza, R., Vizán, H., Zaffarana, C.B., Taylor, G.K., Haller, M., Fernández, R., 2019. Tectonophysics, Volume 750, Pages 45-55. https://doi.org/10.1016/j.tecto.2018.10.028.
Halvorsen, E., 1989. A paleomagnetic pole position of Late Jurassic/Early Cretaceous dolerites from Hinlopenstretet, Svalbard, and its tectonic implications. Earth Planet. Sci. Lett. 94, 398–408.
Hargraves, R.B., 1989. Paleomagnetism of Mesozoic kimberlites in southern Africa and the Cretaceous apparent polar wander curve for Africa. J. Geophys. Res. 94, 1851–1866.
Hargraves, R.B., Rehacek, J., Hooper, P.R., 1997. Palaeomagnetism of the Karoo igneous rocks in southern Africa. S Afr J Geol 100, 195–212.
Hoye, G.S., Evans, M.E., 1975. Remanent magnetization in oxidized olivine. Geophys. J. R. Astr. Soc. 41, 139–151.
Ketelaar, A.C.R., 1963. The direction of the remanent magnetisation in some TD's in SW Greenland, Map Sheets 6O-V-l/61-V1. Greenland Geol. Surv, Copenhagen.
Kent, D. V., Irving, E., 2010. Influence of inclination error in sedimentary rocks on the Triassic and Jurassic apparent polar wander path for North America and implications for Cordilleran tectonics. J. Geophys. Res., 115, B10103, doi:10110.11029/12009JB007205.
Kent, D.V., Kjarsgaard, B.A., Gee, J.S., Muttoni, G., Heaman, L.M., 2015. Tracking the Late Jurassic apparent (or true) polar shift in U-Pb-dated kimberlites from cratonic North America (Superior Province of Canada). Geochem., Geophys Geosyst. 16, 983–994. https://doi.org/10.1002/2015GC005734.
Kent, D.V., Muttoni, G., 2020. Pangea B and the Late Paleozoic Ice Age. Palaeogeogr. Palaeoclimatol. Palaeoecol. 553. https://doi.org/10.1016/j.palaeo.2020.109753.
King, R.F., 1955. The remanent magnetism of artificially deposited sediments. Mon. Not. R. Astr. Soc Geophys. Supp. 7, 115–134.
Kirschvink, J.L., 1980. The least-squares line and plane and the analysis of palaeomagnetic data. Geophys. J. Int. 62, 699–718.
Kodama, K.P., 2009. Simplification of the anisotropy-based inclination correction technique for magnetite- and hematite bearing rocks: a case study for the Carboniferous Glenshaw and Mauch Chunk formations, North America. Geophys. J. Int. 176, 467–477.
Larsen, L.M., Rex, D.C., Watt, W.S., Guise, P.G., 1999. ^{40}Ar–^{39}Ar dating of alkali basaltic dikes along the south-west coast of Greenland: Cretaceous and Tertiary igneous activity along the eastern margin of the Labrador Sea. Geol. Greenland Surv. Bull. 184, 19–29.
Larsen, L.M., Heaman, L.M., Creaser, R.A., Duncan, R.A., Frei, R., Hutchinson, M., 2009. Tectonomagmatic events during stretching and basin formation in the Labrador Sea and the Davis Strait: evidence from age and composition of Mesozoic to Palaeogene dike swarms in West Greenland. J. Geol. Soc. London 166, 999–1012. https://doi.org/10.1144/0016-76492009-038.
Le Breton, E., Handy, M.R., Molli, G., Ustaszewski, K., 2017. Post-20 Ma motion of the Adriatic Plate: New constraints from surrounding orogens and implications for crust-mantle decoupling. Tectonics, 36(12): 3135-3154.Le Maitre, R.W., 2002. Igneous rocks: A classification and glossary terms 2nd Ed. Cambridge University Press. ISBN-10 0-521-66215-X.
Løvlie, R., Torsvik, T.H., 1984. Magnetic remanence and fabric properties of laboratorydeposited hematite bearing red sandstone. Geophys. Res. Lett. 11, 221–224.
McElhinny, M.W., McFadden, P.L., 2000. In: Paleomagnetism: continents and oceans. Academic Press, San Diego, Ca, p. 386 pp..
McEnroe, S., 1996a. A Barremian-Aptian (Early Cretaceous) North American paleomagnetic reference pole. J. Geophys. Res. 101 (B7), 15819–15835.
McEnroe, S., 1996b. North America during the Lower Cretaceous: new palaeomagnetic constraints from intrusions in New England. Geophys. J. Int. 126 (2).
McFadden, P.L., Jones, D.L., 1981. The fold test in palaeomagnetism. Geophys. J. R. Astr. Soc. 67, 53–58.
McFadden, P.L., McElhinny, M., 1990. Classification of the reversal test in palaeomagnetism. Geophys. J. Int. 103, 725–729.
McFadden, P.L., Merrill, R.T., McElhinny, M.W., Lee, S., 1991. Reversals of the Earth's magnetic field and temporal variations of the dynamo families. J. Geophys. Res. 96 (B3), 3923–3933. https://doi.org/10.1029/90JB02275.
Meert, J.G., Pivarunas, A.F., Evans, D.A.D., Pisarevsky. S.A., Pesonen, L.J., Li., Z.X., Elming, S., Millera, S.R., Zhang, S., Salminen, J.M., 2020. The magnificent seven: a proposal for modest revision of the Van der Voo (1990) quality index. Tectonophysics 790, 228549.
Muttoni, G., Erba, E., Kent, D.V., Bachtadse, V., 2005. Mesozoic Alpine facies deposition as a result of past latitudinal plate motion. Nature 434, 59–63.
Muttoni, G., Dallanave, E., Channell, J.E.T., 2013. The drift history of Adria and Africa from 280 Ma to present, Jurassic true polar wander, and zonal climate control on Tethyan sedimentary facies. Palaeogeogr. Palaeoclimatol. Palaeoecol. 386, 415–435. https://doi.org/10.1016/j.palaeo.2013.06.011.
Muttoni, G., Kent, D.V., 2019. Jurassic monster polar shift confirmed by sequential paleopoles from Adria, promontory of Africa. J. Geophys. Res. Solid Earth 124, 3288–3306. https://doi.org/10.1029/2018JB017199.
Nejbert, K., Krajewski, K.P., Dubinska, E., Pecskay, Z., 2011. Dolerites of Svalbard, north-west Barents Sea Shelf: age, tectonic setting and significance for geotectonic interpretation of the High-Arctic Large Igneous Province. Polar Res. 30, 7306. https://doi.org/10.3402/polar.v30i0.7306.
Owen-Smith, T.M., Ganerød, M., van Hinsbergen, D.J.J., Gaina, C., Ashwal, L.D., Torsvik, T.H., 2019. Testing Early Cretaceous Africa-South America fits with new palaeomagnetic data from the Etendeka Magmatic Province (Namibia). Tectonophysics 760, 23–35.
Piper, J.D.A., 1975. A palaeomagnetic study of the coast-parallel Jurassic dyke swarm in southern Greenland. Phys. Earth Planet. Int. 11, 36–42.
Polteau, S., Hendriks, B.W.H., Planke, S., Ganerød, M., Corfu, F., Faleide, J.I., Midtkandal, I., Svensen, H.S., Myklebust, R., 2016. The Early Cretaceous Barents Sea Sill Complex: Distribution, $^{40}Ar/^{39}Ar$ geochronology, and implications for carbon gas formation. Palaeogeogr. Palaeoclimatol. Palaeoecol. 441, 83–95.
Renne, P.R., Mundil, R., Greg Balco, G., Min, K., Ludwig, K.R., 2010. Joint determination of 40K decay constants and $^{40}Ar/^{40}K$ for the Fish Canyon sanidine standard, and improved accuracy for $^{40}Ar/^{39}Ar$ geochronology. Geochim. et Cosmochim. Acta 74, 5349–5367.
Roest, W.R., Danobeitia, J.J., Verhoef, J., Collette, B.J., 1992. Magnetic anomalies in the Canary Basin and the Mesozoic evolution of the central North Atlantic. Mar. Geophys. Res. 14, 1–24. https://doi.org/10.1007/BF01674063.
Solano, M., Goguitchaichvili, A., Sánchez Bettucci, L., Ruiz, R., Calvo-Rathert, M., Ruiz-Martinez, V., Soto, R., Alva-Valdivia, L., 2010. Paleomagnetism of Early Cretaceous Arapey Formation (Northern Uruguay). Stud. Geophys. Geod. 54 (4), 533–546. https://doi.org/10.1007/s11200-010-0032-8.
Steiger, R.H., Jäger, E., 1977. Subcommission on geochronology: convention on the use of decay constants in geo- and cosmochronology. Earth Planet. Sci. Lett. 36, 359–362.
Steinberger, B., Torsvik, T.H., 2008. Absolute plate motions and True Polar Wander in the absence of hotspot tracks. Nature 452, 620–623.
Steinberger, B., Torsvik, T. H.T., 2010. Toward an explanation for the present and past locations of the poles. Geochem., Geophys., Geosyst., 11.
Steiner, M.B., Helsley, C.E., 1975. Reversal pattern and apparent polar wander for the Late Jurassic. Geol. Soc. Am. Bull. 86, 1537–1543.
Steiner, M.B., 2003. A cratonic Middle Jurassic paleopole: Callovian-Oxfordian stillstand (J-2 cusp), rotation of the Colorado Plateau, and Jurassic North American apparent polar wander. Tectonics 22, 3.
Tappe, S., Foley, S.F., Jenner, G.J., Kjarsgaard, B.A., 2005. Integrating ultramafic lamprophyres into the IUGS classification of igneous rocks: rationale and implications. J. Petrol. 46, 1893–1900.
Tauxe, L., Kent, D.V., 1984. Properties of a detrital remanence carried by haematite from study of modern river deposits and laboratory redepositiomn sediments. Geophys. J. R. Astr. Soc. 76, 543–561.
Tauxe, L., Kent, D.V., 2004. A simplified statistical model for the geomagnetic field and the detection of shallow bias in paleomagnetic inclinations: was the ancient magnetic field dipolar? In: Channell, J.E.T., Kent, D., Lowrie, W., Meert, J. G. (Eds.), Timescales of the paleomagnetic field: Geophys. Monogr. Ser., 145. AGU, Washington, DC, pp. 101–117.
Tauxe, L., Kodama, K.P., Kent, D.V., 2008. Testing corrections for paleomagnetic inclination error in sedimentary rocks: a comparative approach. Phys. Earth Planet. Int. 169, 152–165.
Tauxe, L., Shaar, R., Jonestrask, L., Swanson-Hysell, N.L., Minnett, R., Koppers, A.A.P., Constable, C.G., Jarboe, N., Gaastra, K., Fairchild, L., 2016. PmagPy: Software

package for paleomagnetic data analysis and a bridge to the Magnetics Information Consortium (MagIC). Database. Geochem., Geophys., Geosyst. 17. https://doi.org/10.1002/2016GC006307.

Torsvik, T.H., Müller, R.D., Van der Voo, R., Steinberger, B., Gaina, C., 2008. Global plate motion frames: toward a unified model. Rev. Geophys. 46, RG3004. https://doi.org/10.1029/2007RG000227.

Torsvik, T.H., Van der Voo, R., Preeden, U., Mac Niocaill, C., Stinberger, B., Doubrovine, P.V., Van Hinsbergen, D.J.J., Domeier, M., Gaina, C., Tohver, E., 2012. Phanerozoic polar wander, palaeogeography and dynamics, Earth Sci. Rev. 114, 325–368.

Torsvik, T.H.T., Van der Voo, R., Doubrovine, P.V., Burke, K., Steinberger, B., Ashwal, L.D., Trønnes, R.G., Webb, S.J., Bull, A.L., 2014. Deep mantle structure as a reference frame for movements in and on the Earth. Proc. Natl. Ac. Sci., USA, 111 (24) 8735-8740; DOI:/10.1073/pnas.1318135111.

Torsvik, T.H.T., Cocks, L.R.M., 2017. Earth History and Palaeogeography. Cambridge University Press.

Torsvik, T.H.T., Steinberger, B., Shephard, G.E., Doubrovine, P.V., Gaina, C., Domeier, M., Conrad, C.P., Sager W.W., 2019. Pacific-Panthalassic reconstructions: Overview, errata and the way forward. Geochem., Geophys., Geosyst., 20, 7, 3659-3689, https://doi.org/10.1029/2019GC008402.

Town, C. F., Strauss, J. V., Kinney, S. T., Maclennan, S. A., Bradley, D. C., Olsen, P. E., Schoene, B., Setera, J., 2019, New zircon U-Pb geochronological data from the Moat Volcanics, White Mountains, New Hampshire - Implications for rift and/or plume related magmatism. Geol. Soc. Am. Abs. Programs., ISSN 0016-7592, doi: 10.1130/abs/2019NE-327960. (https://gsa.confex.com/gsa/2019NE/meetingapp.cgi/Paper/327960).

Tsai, V. C., Stevenson, D. J., 2007. Theoretical constraints on true polar wander. J. Geophys. Res., Solid Earth, 112.

Van Fossen, M.C., Kent, D.V., 1990. High-latitude paleomagnetic poles from Middle Jurassic plutons and Moat Volcanics in New England and the controversy regarding Jurassic apparent polar wander for North America. J. Geophys. Res. 95, 17503–17516.

Van Fossen, M.C., Kent, D.V., 1992. Paleomagnetism of 122 Ma Plutons in New England and the mid-Cretaceous paleomagnetic field in North America: True polar wander or large scale differential mantle motion? J. Geophys. Res. 97, 19651–19661.

Van Fossen, M.C., Kent, D.V., 1993. A palaeomagnetic study of 143 Ma kimberlite dikes in central New York State. Geophys. J. Int. 113, 175–185.

Van Hinsbergen, D., Mensink, M., Langereis, C., Maffione, M., Spalluto, L., Tropeano, M., Sabato, L., 2014. Did Adria rotate relative to Africa?. Solid Earth 5 (2), 611.

Van Hinsbergen, D.J., Torsvik, T.H., Schmid, S.M., Maţenco, L.C., Maffione, M., Vissers, R.L., Gürer, D., Spakman, W., 2020. Orogenic architecture of the Mediterranean region and kinematic reconstruction of its tectonic evolution since the Triassic. Gondwana Res. 81, 79–229.

Verwey, E.J.W., 1939. Electronic conduction of magnetite (Fe3O4) and its transition point at low-temperature. Nature 44, 327–328.

Van der Voo, R., 1990. The reliability of paleomagnetic data. Tectonophysics 184, 1–9.

Van der Voo, R., 1992. Jurassic paleopole controversy: contributions from the Atlantic bordering continents. Geology 20, 975–978.

Van der Voo, R., Van Hinsbergen, D.J., Domeier, M., Spackman, W., Torsvik, T.H., 2015. Latest Jurassic–earliest Cretaceous closure of the Mongol-Okhotsk Ocean: a paleomagnetic and seismological-tomographic analysis. Geol. Soc. Am. Spec. Pap. 513. https://doi.org/10.1130/2015.2513(19).

Watson, G.S., Enkin, R.J., 1993. The fold test in paleomagnetism as a parameter estimation problem. Geophys. Res. Lett. 20, 2135–2137.

Watt, S.W., 1969. The coast-parallel dike swarm of southwest Greenland in relation to the opening of the Labrador Sea. Can. J. Earth Sci. 6–5. https://doi.org/10.1139/e69-133.

Westphal, M., Montigny, R., Thizat, R., Bardon, C., Bossert, A., Hamzeh, R., 1979. Paléomagnétisme et datation du volcanisme permien, triasique et crétacé du Maroc. Can. J. Earth Sci. 16, 2150–2163.

Yi, Z., Liu, Y., Meert, J.G., 2019. A true polar wander trigger for the Great Jurassic East Asian Aridification. Geology 7 (12), 1112–1116. https://doi.org/10.1130/G46641.1.

Yi, Z., Meert, J.G., 2020. A Closure of the Mongol-Okhotsk Ocean by the Middle Jurassic: Reconciliation of Paleomagnetic and Geological Evidence. Geophys. Res. Lett. 47, 15. https://doi.org/10.1029/2020GL088235.

Zhang, S., Gao, Y., Ren, Q., 2020. Enigma of the Jurassic monster shift of the North China block. Abstract EGU2020-12816. https://doi.org/10.5194/egusphere-egu2020-12816. Link to presentation: EGU2020-12816_presentation.pdf (copernicus.org).